Quantum Monte Carlo Methods and Its Application to Fermi Liquid Theory

by

Anish Ravi Verma

A Thesis

Presented to

The University of Guelph

In partial fulfilment of requirements

for the degree of

Master of Science

in

Physics

Guelph, Ontario, Canada

ABSTRACT

QUANTUM MONTE CARLO METHODS AND ITS APPLICATION TO FERMI LIQUID THEORY

Anish Ravi Verma
University of Guelph, 2022

Advisor:
Professor Alexandros Gezerlis

In this work, the framework of Fermi Liquid Theory was applied to infinite neutron matter. In applying the framework to neutrons interacting through the strong force, care was given to the interactions involved, as the applicability of this framework was probed, given the non-perturbative nature of the strong force.

As input to the calculations, Quantum Monte Carlo calculations were applied to retrieve the energies for neutrons interactive through 2 and 3 body nuclear interactions. In particular, Variational Monte Carlo was used to first optimize the wavefunction, then Auxiliary Field Diffusion Monte Carlo was applied to provide accurate and precise ab-initio energies.

By combining Fermi Liquid Theory and Quantum Monte Carlo methods, we demonstrated a systematization to the calculation of observable parameters, including effective mass, compressibility, spin susceptibility, and g-factor for neutron matter at the thermodynamic limit.

This is particularly relevant for nuclear astrophysics, where neutron stars may be modeled as nuclear matter with a thermodynamic number of neutrons.

Acknowledgements

I dedicate this to my late uncle Harish Narayan Sharma and my late grandmother Satya Bhama Sharma. More than anything, I wish I were able to show you this work.

I am extremely grateful to my family and friends who have given nothing but support and kindness throughout this time. Thank you to Char for your love and support.

Over the last two years, I've been able to learn so much and grow significantly as a person. None of this would have been possible without the guidance of my supervisor Alex Gezerlis, whose wisdom, support, and mentorship have proved invaluable to me. Further, I give my sincere thanks to Andrew Milne and the team at 1QBit for their support and guidance for the past year.

This work was supported by the Natural Sciences and Engineering Research Council (NSERC) of Canada through the Canada Graduate Scholarships-Master's Program, as well as by the Mitacs Accelerate program. Computational resources were provided by SHARCNET, NERSC, and Compute Canada.

Contents

ABSTRACT **ii**

Acknowledgements **iii**

1 Introduction **1**

1.1 Quantum Many Body Systems 1

1.2 The Nuclear Interaction 4

2 Quantum Many-Body Methods **6**

2.1 The Nuclear Many-Body Problem 6

2.2 Monte Carlo Integration 8

2.2.1 Importance Sampling and Monte Carlo Integration 8

2.2.2 Metropolis Algorithm 10

2.3 Variational Monte Carlo Method 13

2.4 Diffusion Monte Carlo Method 15

2.4.1 Fermion Sign Problem 20

2.5 Auxiliary Field Diffusion Monte Carlo Method 22

2.5.1 Fermion Phase Problem 23

2.6 Trial Wavefunction 24

3 Fermi Liquid Theory and its Application to Infinite Nuclear Matter 26

3.1 The Free Fermi Gas 26

3.2 Fermi Liquid Theory 32

3.3 Extending to the Thermodynamic Limit 37

3.3.1 Effective Mass 46

3.3.2 Compressibility 53

3.3.3 Spin Susceptibility 54

3.3.4 Observables for Interacting Neutron Matter 56

4 Conclusion and Outlook 58

Bibliography 60

List of Tables

3.1 Comparison of Integration Methods 41

3.2 Fermi Liquid Theory Observables 56

List of Figures

3.1 Finite size dependence of the free Fermi gas 30

3.2 Landau Interaction Functions for $N = 66$ Interacting Neutrons 39

3.3 Comparing Landau Interaction Functions at the Thermodynamic Limit and at the Finite $N = 66$ Particle Regime 40

3.4 Landau Interaction Functions for $N = 54$ Interacting Neutrons 42

3.5 Landau Interaction Functions for Interacting Neutrons at the Thermodynamic Limit 43

3.6 Dispersion Relation for Interacting Neutrons 49

3.7 Interacting Neutron Effective Mass Ratios as a Function of Number Density 50

Chapter 1

Introduction

1.1 Quantum Many Body Systems

A many-body system in physics is a system of N interacting bodies, where N is typically 3 or greater. A two-body system is often either solvable analytically, or with low computational complexity if the solution is found numerically. This is broadly true for simple classical and quantum systems, respectively. However, often the system of interest involve more interacting pieces than 2 bodies, making them more complex systems that require greater effort to solve.

Historically, calculations involving the interaction of many-body systems have posed great difficulty, because of the increasing computational complexity associated with each added particle. In particular for strongly correlated quantum systems, the dimensionality of the Hilbert space grows exponentially with the system size, and thus the so does the information required for characterizing any state of the system [1, 2, 3]. As a result, the computational power and time required to perform calculations about these systems is large [4]. However, despite the difficulty, there is great interest in making these problems tractable, as they can shed light into a

wide variety of problems like drug discovery and design [5, 6], material design and synthesis [7, 8], astrophysical processes [9, 10], and more.

To get around these issues, one can construct approximate theories that reduce the number of degrees of freedom required to solve the system. A popular regime for this lies in the family of mean-field theory techniques. In essence, mean-field theory maps the many degrees of freedom involved in a many-body problem by constructing a model Hamiltonian which captures the features of the system carrying the most weight in defining the dynamics of the system [11]. The model Hamiltonians involved in various mean-field theories can be heuristic, based on experimental data, or from a more first-principles approach. However, the trade-off for easier computational complexity are errors due to numerical approximation [12] and statistical errors, which can lead to systematic errors in observable calculations and thus the modeling of the system.

There has been much work done to overcome these issues, like with relativistic mean-field theories which have seen some success in calculating observables of some nuclei [13], dynamic mean-field theories which can explain more phenomena [14], and exact mean-field theories, like density functional theory, with some of the widest applicability thus far [15]. However, it is worth noting that with density functional theory, the limiting factor is in deriving the exact energy density functional, which in practice means trying to overcome the difficulty of approximating and constraining an accurate energy density functional [16]. Since the properties of quantum systems can vary drastically with a small change in the parameter space – let alone addressing the issue of scaling calculations up to an interacting many-body problem – finding a way to systematically improve density functional theories is extremely difficult and challenges progress.

However, these theories all run into strong shortcomings when exploring the dynamics of strongly correlated and strongly interacting systems. One reason for this is that small changes in the parameter space for a strongly interacting system can lead to significant changes, which are not accurately described by mean field theories. However, advances in computational power and the mathematical sophistication of newer models has led to the success of a first-principles technique, dubbed Quantum Monte Carlo techniques [17]. Because it is a method derived from first-principles, it inherently provides significantly more accuracy than general mean-field approximations [18]. The advantage this brings over other ab-initio techniques is that it can bypass multi-dimensional integrals without difficult mappings by sampling over complicated probability distributions – which are calculated from the wavefunction of the system.

Explicitly, the Quantum Monte Carlo family of techniques sample the quantum many-body wavefunction, bypassing direct numerical integrations that scale difficultly with growing system size. Once again, because it is an exact method that relies on random sampling to solve the many-body Schrödinger equation, the approximations that are needed are generally tunable and thus can be systematized to give nearly exact results. One of the most famous historic examples of this is in finding the ground state for the homogeneous electron gas [19].

Like any Monte Carlo method, Quantum Monte Carlo algorithms rely on the ability to randomly sample a quantity of interest, based on some probability distribution. The method can run into inaccuracies if enough care isn't taken to ensure the sampling follows a random enough process. This is because the samples can be correlated, and thus a bias can be introduced in calculating the quantity of interest, skewing the final averaged result. However, if there is a way to achieve true random

sampling this can be avoided. Quantum computing may provide this as well, as a speedup for Monte Carlo algorithms in general [20].

Now, it is worth noting that for the Quantum Monte Carlo technique, the accuracy of results rely on the accuracy of the trial wavefunction. The wavefunction will be dependent on the potential used in the many-body Schrödinger equation, and how it is evaluated. There are many ways to optimize the evaluation of the wavefunction that aren't directly related to Quantum Monte Carlo, like the variational method, however can be used in the overall Quantum Monte Carlo calculations.

Now up to this point, the discussion of Quantum Monte Carlo and its accuracy has been completely general for a quantum many-body system. This means that the method has the potential to provide accuracy for a general quantum system, and in the literature has been used in a wide variety of studies. It is found success in molecular physics [21, 22, 23, 24, 25], condensed matter [26, 27], astrophysics [28, 29], nuclear physics[30, 31], and more.

1.2 The Nuclear Interaction

Protons and neutrons, collectively dubbed nucleons, are bound systems of quarks interacting through the strong force, mediated by gluons. The interaction between many nucleons – the nuclear force – is propagated by gluons, and overall can be described by quantum chromodynamics. From this theory, the strong force has an effective range on the order of 1 fm, but is stronger at large separation distances (low energy) and weaker at short distances (high energy). This means that the strong force is non-perturbative in the low-energy regime dominating nuclear physics, making it difficult to probe and model for the case of many particles. It is for this reason that

modeling the nuclear interaction is an ongoing process in nuclear physics.

Different models of the nuclear interaction are classified by the energy-regime, because at different energies, there are different model constraints, and different sets of data are used. These different models are demarcated by different types of nuclear potentials, and thus it is important to be mindful of the regime in which one is performing calculations are performed – different potentials may yield different results.

Although the force in question is extremely difficult to model, the interaction can be greatly simplified, while still being mindful of the nuances of the nuclear force. Consider a dilute gas of neutrons at low temperature in the low energy regime. This dilute gas may act similar to a Fermi gas with a weak interaction, with properties largely independent of the details of the interaction. Within this system, scattering can be modeled with purely attractive radial potentials. This description is predicted to apply to a superfluid phase in the inner crust of a neutron star. Other phases of nuclear matter are predicted to exist within the neutron star as the density of matter increases going inwards toward the centre of the star. However, the precise location of the phase transitions and the properties of the phases are of current interest.

This brings us to the interesting question: Is there a way to model interactions within the neutron star accurately, as a precursor to a model that can probe properties as a function of density?

The framework of Landau Fermi Liquid Theory is used here to model the low-lying excitations of neutron matter and calculate the properties therein. This framework will rely on accurate system energies, for which we will use Quantum Monte Carlo techniques to provide an ab-initio, first principles calculation.

Chapter 2

Quantum Many-Body Methods

2.1 The Nuclear Many-Body Problem

The system we aim to study is pure neutron matter at the thermodynamic limit – in other words, a system of N interacting fermions in the limit of N approaching infinity. To describe this quantum many-body system, we may use the non-relativistic, many-body Schrödinger equation

$$\hat{H} \left| \Psi \left(\{ \mathbf{r}_i \} \right) \right\rangle = E \left| \Psi \left(\{ \mathbf{r}_i \} \right) \right\rangle , \tag{2.1}$$

where H is the many-body Hamiltonian, $\left| \Psi \left(\{ \mathbf{r}_i \} \right) \right\rangle$ is the many-body wavefunction of the system which depends on the set of coordinates $\{ \mathbf{r}_i \}$ for the N particles, and E is the corresponding energy. In order to have any hope of solving this complicated equation, we need to first explicate the Hamiltonian of the system:

$$\hat{H} = -\frac{\hbar^2}{2m} \sum_{i=1}^{N} \nabla_i^2 + \sum_i V_i \left(\mathbf{r}_i \right) + \sum_{i<j} V_{ij} \left(\mathbf{r}_i, \mathbf{r}_j \right) + \sum_{i<j<k} V_{ijk} \left(\mathbf{r}_i, \mathbf{r}_j, \mathbf{r}_k \right) + \dots \tag{2.2}$$

Here, the first term is the sum of kinetic energies, and by itself would describe a free Fermi gas (a set of non-interacting fermions). The second term describes an external potential which encapsulates the energy of the configuration of the N particles. The next term describes the 2-body interactions between the fermions, where each V_{ij} depends on a pair of particles' coordinates. Each successive term describes a higher order m-body interaction.

For the case of pure neutron matter we will truncate the sum at the term describing the three-body interactions, and note that there is no external potential, simplifying our Hamiltonian to

$$\hat{H} = -\frac{\hbar^2}{2m}\sum_{i=1}^{N}\nabla_i^2 + \sum_{i<j} V_{ij}\left(\mathbf{r}_i, \mathbf{r}_j\right) + \sum_{i<j<k} V_{ijk}\left(\mathbf{r}_i, \mathbf{r}_j, \mathbf{r}_k\right). \tag{2.3}$$

The two-body potential we will use is the Argonne V8' (AV8') potential, an approximation of the AV18 potential, and the three-body potential will be the Urbana IX (UIX) potential. The details of these potentials are explained in other works [32, 33, 34, 35, 30]. For the purposes of this work, it is more important to note that both of these are phenomenological potentials, which have been demonstrated to give accurate results [32, 33, 35, 30, 36, 37, 38].

This many-body Schrödinger equation is extremely difficult to solve using ab-inito, microscopic methods [39, 40], and requires significant computational power in order to get results in a reasonable amount of time [41, 42]. This may be alleviated by the use of approximate theories, like mean-field approximations or more phenomenological models, which significantly reduce the computational complexity [43, 11]. By construction, the trade-off for reducing the computational complexity in solving the

problem by employing these approximate theories is the loss of accuracy in comparison to the results from microscopic theories [44].

Luckily, in recent years there has been an explosion in both computing power as well as the sophistication of computational methods used to solve quantum many body problems using microscopic, ab-initio frameworks [40]. This has allowed the extremely accurate description of systems that were previously either difficult or impossible, due to the debilitating complexity of the systems.

One family of methods in particular that has found great success in condensed matter physics [45, 46, 47, 48], chemical physics [49, 50, 51, 52], and nuclear physics [53, 54, 31, 55] are Quantum Monte Carlo methods. In this work, we rely on the Auxiliary Field Diffusion Monte Carlo method to calculate the energy per particle of the system, for which the initial trial wavefunction is optimized by use of the Variational Monte Carlo method.

2.2 Monte Carlo Integration

In order to understand the Variational and Auxiliary Field Diffusion Monte Carlo methods, we first need to understand how to perform a simple Monte Carlo integration.

2.2.1 Importance Sampling and Monte Carlo Integration

In order to perform an d-dimensional integral numerically, there are many methods to be employed, however they all have certain errors associated with them. Simpson's Method for example has an error that goes as $M^{-\frac{4}{d}}$ for M mesh points. The Monte Carlo method of integration, in its statistical foundations, has an error that decreases

as $\sqrt{N}$, where N is the number of points sampled to evaluate the integral, which has the benefit of being independent of d.

With this motivation, let us consider the definite integral of some d-dimensional function $g(\mathbf{R})$ which we wish to evaluate, where $\mathbf{R}$ is the set of coordinates,

$$I = \int g(\mathbf{R}) \mathrm{d}\mathbf{R}. \tag{2.4}$$

Let us now introduce a function $\mathcal{P}(\mathbf{R})$ such that

$$I = \int f(\mathbf{R}) \mathcal{P}(\mathbf{R}) \mathrm{d}\mathbf{R} \tag{2.5}$$

$$f(\mathbf{R}) = \frac{g(\mathbf{R})}{\mathcal{P}(\mathbf{R})} \tag{2.6}$$

in which $\mathcal{P}(\mathrm{R})$ is normalized to 1, and is always positive. This choice allows us to equate our original integral I to the integral of function $f(\mathbf{R})$ weighted by a probability density, or importance function, $\mathcal{P}(\mathbf{R})$. Thus, the integral I may be approximated by sampling N values of $f(\mathbf{R})$ over a set of $\mathbf{R}_i$ distributed according to the importance function. Writing this explicitly,

$$I = \lim_{N \to \infty} \frac{1}{N} \sum_{i=1}^{N} f(\mathbf{R}_i) \tag{2.7}$$

$$I \approx \frac{1}{N} \sum_{i=1}^{N} f(\mathbf{R}_i). \tag{2.8}$$

The corresponding variance to this approximation is

$$\frac{\sigma^2}{N} = \frac{1}{N(N-1)} \sum_{i=1}^{N} \left(f(\mathbf{R}_i) - \frac{1}{N} \sum_{j=1} f(\mathbf{R}_j) \right)^2, \tag{2.9}$$

where we have an $N - 1$ on the right hand side as we are taking a finite sample, as

opposed to the infinite population required to get the exact result for the integral.

This technique to randomly sample points in the above evaluation of the integral is dubbed "Importance Sampling" [56, 57], and will allow us to relate the upcoming methods back to this simple Monte Carlo method of integration through the importance function. In general a conscious choice of the importance function needs to be made to reduce the variance obtained. The minimal variance [56] will be given by an importance function of

$$\mathcal{P}(\mathbf{R}) = \left| \frac{g(\mathbf{R})}{I} \right|. \tag{2.10}$$

The value of I is unknown–recall that we are employing this integration technique in order to evaluate I–which means that the variance minimizing importance function is unknown. However, by using this method iteratively, optimizing the importance function based on the results of the previous iteration, a more accurate and precise result, since the variance is reduced, is obtained.

This idea is that the importance function determines the quality of the result is going to be crucial in practice and should be remembered for the upcoming sections.

2.2.2 Metropolis Algorithm

The importance sampling technique above relied on us being able to make use of a normalized importance function. However, if the importance function is extremely difficult to normalize, then our methodology discussed thus far fails.

To alleviate this issue, we may employ the Metropolis algorithm [58] to sample points. This algorithm cares about the ratio of importance functions for two different configurations, which cancels out the dependence on the normalization. The details of this algorithm are as follows.

First, we define a walker as some configuration $\mathbf{R}$, which is set to move or "walk" to a new configuration after some step. Consider a walker initially at a configuration $\mathbf{R}$ which makes a trial step to a new configuration $\mathbf{R}'$, which is determined from a probability density function $T(\mathbf{R}' \leftarrow \mathbf{R})$. To get the total probability of this trial step, we simply need to scale the probability density function by the relevant volume element $\mathrm{d}\mathbf{R}'$ and the probability of accepting this trial step $A(\mathbf{R}' \leftarrow \mathbf{R})$, as

$$\mathcal{P}(\mathbf{R})\mathrm{d}\mathbf{R}' = T(\mathbf{R}' \leftarrow \mathbf{R})A(\mathbf{R}' \leftarrow \mathbf{R})\mathrm{d}\mathbf{R}', \tag{2.11}$$

where we take

$$A(\mathbf{R}' \leftarrow \mathbf{R}) = \mathrm{Min}\left(1, \frac{T(\mathbf{R} \leftarrow \mathbf{R}')\mathcal{P}(\mathbf{R}')}{T(\mathbf{R}' \leftarrow \mathbf{R})\mathcal{P}(\mathbf{R})}\right). \tag{2.12}$$

What is commonly done is to take the ratio $T(\mathbf{R} \leftarrow \mathbf{R}')/T(\mathbf{R}' \leftarrow \mathbf{R})$ to be unity, leading to

$$A(\mathbf{R}' \leftarrow \mathbf{R}) = \mathrm{Min}\left(1, \frac{\mathcal{P}(\mathbf{R}')}{\mathcal{P}(\mathbf{R})}\right). \tag{2.13}$$

Now, if we consider a walker density of $n(\mathbf{R})$, we can modify the probability to give the average number of walkers going from $\mathbf{R}$ to $\mathbf{R}'$ in a single step as

$$n(\mathbf{R})\mathrm{d}\mathbf{R}T(\mathbf{R}' \leftarrow \mathbf{R})A(\mathbf{R}' \leftarrow \mathbf{R})\mathrm{d}\mathbf{R}'. \tag{2.14}$$

Now, it is expected that the average number of walkers going from $\mathbf{R}$ to $\mathbf{R}'$ to be balanced out by the average number of walkers going from $\mathbf{R}'$ to $\mathbf{R}$. This balance condition goes as

$$n(\mathbf{R}')\mathrm{d}\mathbf{R}'T(\mathbf{R} \leftarrow \mathbf{R}')A(\mathbf{R} \leftarrow \mathbf{R}')\mathrm{d}\mathbf{R} = n(\mathbf{R})\mathrm{d}\mathbf{R}T(\mathbf{R}' \leftarrow \mathbf{R})A(\mathbf{R}' \leftarrow \mathbf{R})\mathrm{d}\mathbf{R}', \tag{2.15}$$

which after rearranging leads to

$$\frac{n(\mathbf{R})}{n(\mathbf{R}')} = \frac{T(\mathbf{R} \leftarrow \mathbf{R}')A(\mathbf{R} \leftarrow \mathbf{R}')}{T(\mathbf{R}' \leftarrow \mathbf{R})A(\mathbf{R}' \leftarrow \mathbf{R})}. \tag{2.16}$$

By substituting Eq. (2.11) , we obtain

$$\frac{n(\mathbf{R})}{n(\mathbf{R}')} = \frac{\mathcal{P}(\mathbf{R})}{\mathcal{P}(\mathbf{R}')}, \tag{2.17}$$

thus leading to the result that the probability of finding a walker in a given volume element is given by $\mathcal{P}(\mathbf{R})\mathrm{d}\mathbf{R}$.

This derivation demonstrates two things. First, the walkers become distributed according to the importance function the number of steps made approach infinity. Second is that this method utilizes the ratio of the importance functions at different configurations, meaning that the issue of normalization is solved, as the normalizing factor cancels.

Now, there are some subtleties that a keen eye may have caught. The above explication ends in the result that the distribution of walkers approach $\mathcal{P}(\mathbf{R})$. However, this if there are other possible distributions to approach other than $\mathcal{P}(\mathbf{R})$, then it is required to be shown that this process will indeed approach $\mathcal{P}(\mathbf{R})$ and not some other distribution. In fact, this is already guaranteed by the nature of this process, as it is an ergodic, discrete Markov chain process. With ergodic Markov chain processes, there exists a unique stationary distribution, which the walkers approach after an infinite number of steps, which was demonstrated to be $\mathcal{P}(\mathbf{R})$ above.

Another problem that needs to be addressed is the autocorrelation between successive walker configurations. To explore this, we can introduce an acceptance ratio. This ratio is simply the number of trial steps that were accepted divided by the total

number of trial steps. If the proposed steps are very large in size, then it is expected that there will be very many rejections for the proposed trial steps, and a small acceptance ratio. With this small acceptance ratio, the walkers won't move around very much in the phase space, and as a result, the set of walker configurations will be highly autocorrelated. Similarly, a small trial step size resulting in a large acceptance ratio also results in highly autocorrelated walker configurations. However, now the cause is due to the large number of steps required to cover an adequate region of phase space. Thus, an acceptance ratio of $\sim 50\%$ is desirable to reduce the problem of autocorrelation.

2.3 Variational Monte Carlo Method

The Variational Monte Carlo method makes use of the variational principle from quantum mechanics. This principle states that the expectation value of a Hamiltonian $\hat{H}$ using some trial wavefunction Ψ_{T} is greater than or equal to the true ground state energy of the system E_0 corresponding to the Hamiltonian; explicitly

$$E_0 \leq \frac{\Psi_{\mathrm{T}}^* \hat{H} \Psi_{\mathrm{T}}}{\Psi_{\mathrm{T}}^* \Psi_{\mathrm{T}}}. \tag{2.18}$$

However, for the right hand side of Eq. (2.18) to equal the ground state, the trial wavefunction has to be the true ground state of the system. Effectively, this tells us that the more similar the trial wavefunction is to the ground state wavefunction, the better a result will be obtained for the energy of the system. Already, this sounds analogous to the choice of importance function in the simple Monte Carlo integration

described previously. With this in mind, let us recast Eq. (2.18) as

$$E_0 \leq \frac{\int \Psi_{\mathrm{T}}^* \hat{H} \Psi_{\mathrm{T}} \mathrm{d}\mathbf{R}}{\int \Psi_{\mathrm{T}}^* \Psi_{\mathrm{T}} \mathrm{d}\mathbf{R}} \tag{2.19}$$

$$E_0 \leq \frac{\int \Psi_{\mathrm{T}}^* \Psi_T \Psi_{\mathrm{T}}^{-1} \hat{H} \Psi_{\mathrm{T}} \mathrm{d}\mathbf{R}}{\int \Psi_{\mathrm{T}}^* \Psi_{\mathrm{T}} \mathrm{d}\mathbf{R}} \tag{2.20}$$

$$E_0 \leq \int \frac{|\Psi|^2}{\int \Psi_{\mathrm{T}}^* \Psi_{\mathrm{T}} \mathrm{d}\mathbf{R}} \Psi_{\mathrm{T}}^{-1} \hat{H} \Psi_{\mathrm{T}} \mathrm{d}\mathbf{R} \tag{2.21}$$

$$E_0 \leq \int \mathcal{P}(\mathbf{R}) E_{\mathrm{L}}(\mathbf{R}) \mathrm{d}\mathbf{R}, . \tag{2.22}$$

The form of Eq. (2.22) is that of Eq. (2.5), where the integrand to be evaluated is

$$E_{\mathrm{L}}(\mathbf{R}) = \Psi_{\mathrm{T}}^{-1} \hat{H} \Psi_{\mathrm{T}} \tag{2.23}$$

with an importance function of

$$\mathcal{P}(\mathbf{R}) = \frac{|\Psi_T(\mathbf{R})|^2}{\int |\Psi_T(\mathbf{R})|^2 \mathrm{d}\mathbf{R}} \mathrm{d}\mathbf{R}, \tag{2.24}$$

which allows us to employ Monte Carlo Integration using importance sampling and the Metropolis algorithm in order to evaluate the integral. Once again, the normalization of the importance function does not matter in the random sampling according to the importance function, as the Metropolis algorithm deals with ratios of the importance function. The importance of this cannot be overstated, as the normalization for the large many-body wavefunction may prove difficult to compute. Thus, the variational energy may be evaluated as

$$E \approx \frac{1}{N} \sum_{i=1}^{N} E_{\mathrm{L}}(\mathbf{R}_i). \tag{2.25}$$

Once again, this energy will provide an upper bound on the true ground state energy. By how much this variational energy differs from the true ground state energy depends

on how close the trial wavefunction is to the true ground state wavefunction.

2.4 Diffusion Monte Carlo Method

It is instructive to understand the basics of Diffusion Monte Carlo before proceeding to Auxiliary Field Diffusion Monte Carlo. The main property of Schrödinger's equation that is the conceptual basis for this method is the fact that the time-dependent wavefunction can be expanded out in terms of the time-independent basis states, weighted by expansion coefficients and the time evolution operator. Using a careful choice of parameters, this property can be used to project out and yield the ground state of the Hamiltonian. This method belongs to a class of methods called "projector methods", and for our purposes is used to solve the imaginary-time, many-body Schrödinger's equation

$$-\frac{\partial}{\partial\tau}\Psi(\mathbf{R},\tau) = (\hat{H} - E_{\mathrm{T}})\Psi(\mathbf{R},\tau), \tag{2.26}$$

where τ is the imaginary time, which in terms of the real time t is defined as $\tau = it/\hbar$, and E_{T} is some advantageous shift in the zero energy. Now, if this equation is rewritten by expanding the Hamiltonian operator and denote $\hbar^2/(2m)$ as D,

$$\frac{\partial}{\partial\tau}\Psi(\mathbf{R},\tau) = \left(D\nabla^2 + (-V + E_T\right)\Psi(\mathbf{R},\tau). \tag{2.27}$$

Note that in Eq. (2.27), the first term on the right-hand side when equated to the left-hand side is simply the diffusion equation, while the second term on the right-hand side when equated to the left-hand side is a rate equation. Effectively, this equation implies that the walkers in our simulations will diffuse and the number of walkers

may grow or decay.

The time evolution of the wavefunction is simply an expansion of the eigenfunctions of the Hamiltonian weighted by the time evolution operator and the expansion coefficients c_i,

$$\Psi(\mathbf{R},\tau) = \sum_{i=0} c_i e^{-(\hat{H}-E_{\mathrm{T}})\tau}\Psi_i(\mathbf{R}) = \sum_{i=0} c_i e^{-(E_i-E_{\mathrm{T}})\tau}\Psi_i(\mathbf{R}). \tag{2.28}$$

In the limit of infinite imaginary time, this directly leads to

$$\lim_{\tau\to\infty}\Psi(\mathbf{R},\tau) = \lim_{\tau\to\infty} c_0 e^{-(E_0-E_{\mathrm{T}})\tau}\Psi_0(\mathbf{R}), \tag{2.29}$$

where if E_T approaches the ground state energy E_0, then the ground state wavefunction is obtained asymptotically. Thus, all we need now is a method by which to solve the imaginary-time Schrödinger's equation in order to obtain the ground state wavefunction. Now, if E_T is greater than E_0 then it is clear that this leads to an exponential growth of the ground state wavefunction, while for an E_T less than E_0, there is a resultant exponential decay of the ground state wavefunction. That is, this is a population growth estimator.

The above discussions give qualitative reasons describing diffusion and branching. In order to obtain a more explicit and quantitative measure of the diffusion and branching, we first recast the wavefunction $\Psi(\mathbf{R},\tau)$ in terms of a time independent trial wavefunction $\Psi_{\mathrm{T}}(\mathbf{R})$ as

$$\Psi(\mathbf{R},\tau) = \int \langle\mathbf{R}|e^{-(\hat{H}-E_{\mathrm{T}})\tau}|\mathbf{R}'\rangle\Psi_{\mathrm{T}}(\mathbf{R}')\mathrm{d}\mathbf{R}', \tag{2.30}$$

where $|\mathbf{R}\rangle$ is the many-body position basis state. This is a non-trivial calculation,

but can be made significantly easier. A property of the time evolution operator $U(\tau)$ is

$$\hat{U}(\tau)\Psi(\mathbf{R}) = \hat{U}(\tau_2)\hat{U}(\tau_1)\Psi(\mathbf{R}) \tag{2.31}$$

for $\tau = \tau_1 + \tau_2$. Thus, we can can recast Eq. (2.30) in terms of M finite timesteps, $\Delta\tau = \tau/M$, as

$$\Psi(\mathbf{R}_M, \tau) = \int \prod_{j=0}^{M-1} G(\mathbf{R}_{j+1}, \mathbf{R}_j) \prod_{i=0}^{M-1} \mathrm{d}R_i, \tag{2.32}$$

where we've denoted the relevant matrix element for the finite-step time evolution operator as

$$G(\mathbf{R}_{j+1}, \mathbf{R}_j) = \langle \mathbf{R}_{j+1} | e^{-(\hat{H} - E_\mathrm{T})\Delta\tau} | \mathbf{R}_j \rangle \tag{2.33}$$

Now we need a tool with which to evaluate this matrix element. Todo this the well-known Strang Splitting [59] is employed, which makes use of the Trotter-Suzuki approximation, as

$$\begin{aligned}
G(\mathbf{R}_{j+1}, \mathbf{R}_j) &= \langle \mathbf{R}_{j+1} | e^{-(\hat{H} - E_\mathrm{T})\Delta\tau} | \mathbf{R}_j \rangle & (2.34)\\
&= \langle \mathbf{R}_{j+1} | e^{-\hat{T}\Delta\tau - (\hat{V} - E_\mathrm{T})\Delta\tau} | \mathbf{R}_j \rangle & (2.35)\\
&\approx \langle \mathbf{R}_{j+1} | e^{-(\hat{V} - E_\mathrm{T})\frac{\Delta\tau}{2}} e^{-(\hat{T})\Delta\tau} e^{-(\hat{V} - E_\mathrm{T})\frac{\Delta\tau}{2}} | \mathbf{R}_j \rangle & (2.36)\\
&= \langle \mathbf{R}_{j+1} | e^{-\hat{T}\Delta\tau} | \mathbf{R}_j \rangle e^{-(V(\mathbf{R}_{j+1}) + V(\mathbf{R}_j) - 2E_\mathrm{T})\frac{\Delta\tau}{2}} & (2.37)\\
G(\mathbf{R}_{j+1}, \mathbf{R}_j) &= G_\mathrm{D}(\mathbf{R}_{j+1}, \mathbf{R}_j) G_\mathrm{B}(\mathbf{R}_{j+1}, \mathbf{R}_j). & (2.38)
\end{aligned}$$

This demonstrates that we can split the Green's function $G(\mathbf{R}_{j+1}, \mathbf{R}_j)$ into a diffusion Green's function $G_\mathrm{D}(\mathbf{R}_{j+1}, \mathbf{R}_j)$ and a branching Green's function $G_\mathrm{D}(\mathbf{R}_{j+1}, \mathbf{R}_j)$, motivated by the form of Eq. (2.27). The diffusion Green's function is not difficult to evaluate, and may be easily evaluated when noting that the inner product of the many-body position basis function $|\mathbf{R}\rangle$ and the many-body momentum basis function

$|\mathbf{P}\rangle$:

$$
\begin{aligned}
G_{\mathrm{D}}(\mathbf{R}_{j+1},\mathbf{R}_j) &= \langle \mathbf{R}_{j+1}|e^{-\hat{T}\Delta\tau}|\mathbf{R}_j\rangle && (2.39)\\
&= \int \langle \mathbf{R}_{j+1}|e^{-\hat{T}\Delta\tau}|\mathbf{P}\rangle\langle\mathbf{P}|\mathbf{R}_j\rangle \mathrm{d}\mathbf{P} && (2.40)\\
&= \int \langle \mathbf{R}_{j+1}|e^{-\hat{T}\Delta\tau}|\mathbf{R}_j\rangle \sqrt{\frac{1}{(2\pi\hbar)^{3N}}} e^{-\frac{i}{\hbar}\mathbf{P}\cdot\mathbf{R}_j}\mathrm{d}\mathbf{P} && (2.41)\\
&= \sqrt{\frac{1}{(2\pi\hbar)^{3N}}}\int \sqrt{\frac{1}{(2\pi\hbar)^{3N}}} e^{-\frac{\mathbf{P}^2}{2m}\Delta\tau} e^{-\frac{i}{\hbar}\mathbf{P}\cdot\mathbf{R}_{j+1}} e^{-\frac{i}{\hbar}\mathbf{P}\cdot\mathbf{R}_j}\mathrm{d}\mathbf{P} && (2.42)\\
&= \frac{1}{(2\pi\hbar)^{3N}}\int e^{-\frac{\mathbf{P}^2}{2m}\Delta\tau - \frac{i}{\hbar}\mathbf{P}\cdot(\mathbf{R}_{j+1}-\mathbf{R}_j)}\mathrm{d}\mathbf{P} && (2.43)\\
G_{\mathrm{D}}(\mathbf{R}_{j+1},\mathbf{R}_j) &= \left(\frac{m}{2\pi\hbar^2\Delta\tau}\right)^{\frac{3N}{2}} e^{-\frac{(\mathbf{R}_{j+1}-\mathbf{R}_j)^2}{2\hbar^2\tau/m}}. && (2.44)
\end{aligned}
$$

Thus, the diffusion Green's function is a Gaussian with a variance $\sigma_D^2 = \frac{\hbar^2\Delta\tau}{m}$

Now, the branching Green's function is typically evaluated using some modified version of the Green's function, as it in general can prove difficult to compute. Since we are building a Monte Carlo method we need to find a means with which to take random samples for the walker configurations. This is achieved using the Gaussian form of $G_D(\mathbf{R}_{j+1},\mathbf{R}_j)$. Typically employed for Diffusion Monte Carlo calculations of energies (and for operators in general) is the mixed estimator of the Hamiltonian

$$\langle\hat{H}\rangle_{\mathrm{M}} = \frac{\langle\Psi(\tau)|\hat{H}|\Psi_{\mathrm{T}}\rangle}{\langle\Psi(\tau)|\Psi_{\mathrm{T}}\rangle}. \qquad (2.45)$$

If we consider the limit of infinite imaginary time, it is clear that the bras approach approach the ground state. However, if we apply the time operator as follows, we will obtain the ground state energy

$$\langle\hat{H}\rangle_{\mathrm{M}} = \frac{\langle\Psi(\tau)|\hat{H}|\Psi_{\mathrm{T}}\rangle}{\langle\Psi(\tau)|\Psi_{\mathrm{T}}\rangle} \qquad (2.46)$$

$$\langle \hat{H} \rangle_{\mathrm{M}} = \frac{\langle \Psi(\tau) | U\left(-\frac{\tau}{2}\right) U\left(\frac{\tau}{2}\right) \hat{H} | \Psi_{\mathrm{T}} \rangle}{\langle \Psi(\tau) | U\left(-\frac{\tau}{2}\right) U\left(\frac{\tau}{2}\right) | \Psi_{\mathrm{T}} \rangle} \tag{2.47}$$

$$\langle \hat{H} \rangle_{\mathrm{M}} = \frac{\langle \Psi\left(\frac{\tau}{2}\right) | \hat{H} | \Psi\left(\frac{\tau}{2}\right) \rangle}{\langle \Psi\left(\frac{\tau}{2}\right) | \Psi\left(\frac{\tau}{2}\right) \rangle} \tag{2.48}$$

$$\Longrightarrow \lim_{\tau \to \infty} \langle \hat{H} \rangle_{\mathrm{M}} = \frac{\langle \Psi_0 | \hat{H} | \Psi_0 \rangle}{\langle \Psi_0 | \Psi_0 \rangle} = E_0. \tag{2.49}$$

Now, consider a more general case in which the operator corresponding to the observable does not commute with the time evolution operator. Then, another approach is needed in order to calculate the estimator. Indeed, if we consider the estimator above in its integral form in terms of the Green's functions, we obtain

$$\langle \hat{H} \rangle_{\mathrm{M}} = \frac{\int \prod_{j=0}^{N-1} G(\mathbf{R}_{j+1}, \mathbf{R}_j) \Psi_{\mathrm{T}}(\mathbf{R}_0) \hat{H} \Psi_{\mathrm{T}}(\mathbf{R}_0) \prod_{i=0}^{N} \mathrm{d}\mathbf{R}_i}{\int \prod_{j=0}^{N-1} G(\mathbf{R}_{j+1}, \mathbf{R}_j) \Psi_{\mathrm{T}}(\mathbf{R}_0) \Psi_{\mathrm{T}}(\mathbf{R}_0) \prod_{i=0}^{N} \mathrm{d}\mathbf{R}_i} \tag{2.50}$$

$$\langle \hat{H} \rangle_{\mathrm{M}} = \frac{\int \frac{\prod_{j=0}^{N-1} G(\mathbf{R}_{j+1}, \mathbf{R}_j) \Psi_{\mathrm{T}}(\mathbf{R}_0) \hat{H} \Psi_{\mathrm{T}}(\mathbf{R}_0)}{\mathcal{W}(\{\mathbf{R}_k\})} \frac{\mathcal{W}(\{\mathbf{R}_k\})}{\int \mathcal{W}(\{\mathbf{R}_k\}) \prod_{l=0}^{N} \mathrm{d}\mathbf{R}_l} \prod_{i=0}^{N} \mathrm{d}\mathbf{R}_i}{\int \frac{\prod_{j=0}^{N-1} G(\mathbf{R}_{j+1}, \mathbf{R}_j) \Psi_{\mathrm{T}}(\mathbf{R}_0) \Psi_{\mathrm{T}}(\mathbf{R}_0)}{\mathcal{W}(\{\mathbf{R}_k\})} \frac{\mathcal{W}(\{\mathbf{R}_k\})}{\int \mathcal{W}(\{\mathbf{R}_k\}) \prod_{l=0}^{N} \mathrm{d}\mathbf{R}_l} \prod_{i=0}^{N} \mathrm{d}\mathbf{R}_i}, \tag{2.51}$$

Both the numerator and the denominator take the familiar form of the Monte Carlo integral discusses above, where the weighting function $\mathcal{W}(\{\mathbf{R}_k\})$ is given by

$$\mathcal{W}(\{\mathbf{R}_k\}) = \prod_{j=0}^{N-1} \left[\Psi_{\mathrm{T}}(\mathbf{R}_{j+1}) G(\mathbf{R}_{j+1}, \mathbf{R}_j) \right] \Psi_{\mathrm{T}}(\mathbf{R_0}) \tag{2.52}$$

$$\mathcal{W}(\{\mathbf{R}_k\}) = \prod_{j=0}^{N-1} \left[\Psi_{\mathrm{T}}(\mathbf{R}_{j+1}) G(\mathbf{R}_{j+1}, \mathbf{R}_j) \Psi^{-1}(\mathbf{R}_j) \right] \Psi_{\mathrm{T}}^2(\mathbf{R_0}) \tag{2.53}$$

where we may rewrite the product in the square bracket in terms of a modified Green's function, $\tilde{G}(\mathbf{R}_{j+1}, \mathbf{R}_j) = \prod_{j=0}^{N-1} \Psi_{\mathrm{T}}(\mathbf{R}_{j+1}) G(\mathbf{R}_{j+1}, \mathbf{R}_j)$, for which the integral of $\mathcal{W}(\{\mathbf{R}_k\})$ over the set of $\{\mathbf{R}_{N-1}\}$ is given by

$$\int \mathcal{W}(\{\mathbf{R}_k\}) \prod_{i=0}^{N-1} \mathrm{d}\mathbf{R}_i = \int \tilde{G}(\mathbf{R}_{j+1}, \mathbf{R}_j) \Psi_{\mathrm{T}}^2(\mathbf{R_0}) \prod_{i=0}^{N-1} \mathrm{d}\mathbf{R}_i \tag{2.54}$$

$$\int \mathcal{W}(\{\mathbf{R}_k\}) \prod_{i=0}^{N-1} \mathrm{d}\mathbf{R}_i \;=\; \Psi(\mathbf{R}_N,\tau)\Psi_{\mathrm{T}}(\mathbf{R}_N). \tag{2.55}$$

Plugging this relation into the form of the estimator in Eq. (2.51), we have

$$\langle \hat{H} \rangle_{\mathrm{M}} = \int \Psi_{\mathrm{T}}^{-1}(\mathbf{R}_N)\hat{H}\Psi_{\mathrm{T}}(\mathbf{R}_N) \frac{\mathcal{W}(\{\mathbf{R}_k\})}{\int \mathcal{W}(\{\mathbf{R}_k\}) \prod_{l=0}^{N} \mathrm{d}\mathbf{R}_l} \prod_{i=0}^{N} \mathrm{d}\mathbf{R}_i \tag{2.56}$$

$$\langle \hat{H} \rangle_{\mathrm{M}} = \int \Psi_{\mathrm{T}}^{-1}(\mathbf{R}_N)\hat{H}\Psi_{\mathrm{T}}(\mathbf{R}_N) \frac{\Psi(\mathbf{R}_N,\tau)\Psi_{\mathrm{T}}(\mathbf{R}_N)}{\int \Psi(\mathbf{R}_N,\tau)\Psi_{\mathrm{T}}(\mathbf{R}_N)\mathrm{d}\mathbf{R}_N} \mathrm{d}\mathbf{R}_N \tag{2.57}$$

$$\langle \hat{H} \rangle_{\mathrm{M}} = \int E_{\mathrm{L}}(\mathbf{R}_N)\mathcal{P}(\mathbf{R}_N,\tau)\mathrm{d}\mathbf{R}_N. \tag{2.58}$$

This final line shows that the estimator is simply a Monte Carlo integral of the local energy, that is distributed according to the importance function

$$\mathcal{P}(\mathbf{R}_N,\tau) = \frac{\Psi(\mathbf{R}_N,\tau)\Psi_{\mathrm{T}}(\mathbf{R}_N)}{\int \Psi(\mathbf{R}_N,\tau)\Psi_{\mathrm{T}}(\mathbf{R}_N)\mathrm{d}\mathbf{R}_N}. \tag{2.59}$$

One interesting thing to note here is that the importance function has a dependence on τ. This effectively means that the effect of sampling walker configurations is equivalent to that of evolving the wavefunction in time. In either method, it is important to make sure that the trial wavefunction is as similar to the ground state wave-function as possible, as discussed earlier for importance sampling to reduce the variance, and to approach the ground state quickly.

2.4.1 Fermion Sign Problem

Before moving on to describing the Auxiliary Field Diffusion Quantum Monte Carlo method, we will address a particular problem that has not explicitly emerged, but plagues quantum Monte Carlo methods in general, with exception of the Variational Monte Carlo method [60]. Being a family of probabilistic methods, quantum

Monte Carlo methods can only handle positive distributions. For systems of fermions, the anti-symmetry of the wavefunction required by the Pauli exclusion principle leads to nodal surfaces–that is, $\Psi = 0$. One naïve attempt to remedy this may come as a generalization of the Diffusion Monte Carlo method in assigning signed weights to the walkers in an attempt to cancel the symmetric portions of the trial wavefunction. This attempt, however, leads to an exponential decay of the signal-to-noise ratio [61], which is a non-trivial problem to solve in general. In fact, it is believed that there may not be a general solution to the fermion sign problem [60, 62].

However, a method that has had success in reducing the errors resulting from this problem is the fixed-node approximation. In this method there is a restriction placed on the walkers, such that if a walker crosses a node, that is if it changes sign after a step, it is killed and removed from the simulation. Alternatively, the walker-move can be rejected if the trial step proposes crossing the nodal surface, as opposed to simply allowing the step and removing the walker after-the-fact which proves to be a better choice [63]. This can be further improved by introducing a guidance function Ψ_{G} that biases the walkers to areas of the phase space where the probability density function of the trial wavefunction is maximized. That is Ψ_{G} should go as $|\Psi_{\mathrm{T}}|^2$ [64]. Hence a fixed-nodal surface, which through the quantum Monte Carlo simulation will produce the lowest energy wavefunction that follows this nodal surface. This nodal surface depends on the the trial wavefunction, once again demonstrating the importance of having a trial wavefunction as close to the ground state as possible in order to obtain accurate results in a shorter imaginary time evolution.

2.5 Auxiliary Field Diffusion Monte Carlo Method

The framework explicated thus far has described a potentials and wavefunctions that depend on positions. However, if there are other dependencies, like spin and isospin, the methodology needs to be modified to be sufficient. For nuclear matter in general, the nuclear potential and interactions involved have many other components that go into them, like spin, isospin, the tensor force interaction, etc. In the Diffusion Monte Carlo method, this amounts to sampling the walker positions and explicitly summing over the spin-isospin states. For each nucleon there are four spin-isospin states. Computationally the sampling of positions is controlled, but the summing of spin-isospin states grows exponentially with the number of nucleons, as 4^N. Note that for pure neutron matter the isospin degree of freedom is fixed, as there are no particles with differing isospin (ie protons). Clearly this is not desirable, and a way to sample spin-isospin states is required. This is accomplished by way of Auxiliary Field Diffusion Monte Carlo, which is one of the most efficient way to accomplish this today [65].

Essentially, the Auxiliary Field Diffusion Monte Carlo method is an extension of the Diffusion Monte Carlo method by evaluating the propagator of G_{B} in a particular way. First, the Hubbard-Stratanovich transformation is used to write the propagator as an integral over some set of auxiliary fields of a product of single-particle spin operators. The auxiliary fields are then sampled, where ultimately the sample independently changes for each spinor for each particle in the sample, resulting in a new sampled walker [65, 66]. Which means, along with G_{D}, both the spin and positions are sampled by the Auxiliary Field Diffusion Monte Carlo method.

2.5.1 Fermion Phase Problem

In analogue to fermion sign problem in the Diffusion Monte Carlo method, there is a fermion phase problem in the case of Auxiliary Field Diffusion Monte Carlo. To see how this arises, consider the form of, for example, the tensor-force

$$3(\hat{r}_{ij} \cdot \sigma_i)(\hat{r}_{ij} \cdot \sigma_j) - \sigma_i \cdot \sigma_j. \tag{2.60}$$

In the above, σ_k represents the Pauli spin matrices indexed over particle number. Because the Pauli matrices are in general complex, the operations involving the Pauli matrices can yield a complex-valued. As the methodology of Auxiliary Field Diffusion Monte Carlo is constructed to handle spin-dependent potentials by sampling terms that involve spin-dependent operators, the trial wave-function evaluated at the walker configurations may be complex in general.

In a similar fashion to the approach the fermion sign problem by means of a fixed-node approximation, the fermion phase problem may be handled by fixed-phase approximation [67]. In this approximation scheme, the path of the walkers is constrained, similarly to how the restraint was imposed in the fixed-node approximation, such that the real part of the wavefunction is positive. If the sign of the real part of the wavefunction is that of the correct ground-state wavefunction, then the correct, exact result is obtained, while small deviations give second order corrections to the energy [66].

2.6 Trial Wavefunction

As has been touched on in each of the methodologies explicated above, the trial wavefunction being as similar to the ground-state wavefunction itself is paramount in the accuracy of the results obtained using Monte Carlo methods. Further, since the trial wavefunction is used in the importance sampling for the variation, diffusion, and Auxiliary Field Diffusion Monte Carlo methods it also controls the statistical efficiency of the simulations. In the two Diffusion Monte Carlo methods, the nodal pockets play an especially important role [60].

In quantum many-body chemistry, a well-known method to obtain the many-body wavefunction is by use of a linear combination of Slater determinants. For quantum Monte Carlo methods in general, a more compact form of the trial wavefunction is desirable and a Slater-Jastrow form is used [68]. This form of the trial wavefunction is most simply expressed as

$$\Psi_{\mathrm{T}} = F_{\mathrm{J}}(\mathbf{R}) D_{\mathrm{S}}(\mathbf{R}, S), \tag{2.61}$$

where $F_{\mathrm{J}}(\mathbf{R})$ is a Jastrow factor and $D(\mathbf{R}, S)$ is a single Slater determinant, where S is the set of spins for the particles involved. The Jastrow factor itself is nodeless, meaning that it only affects the variance of the trial wavefunction and not the nodal surfaces. This factor is chosen to reduce the variance by providing information of the positions of where the particles are biased towards, dictated by the spin-independent parts of the interactions, $v(r)$, through the relation

$$-\frac{\hbar^2}{2m}\nabla^2 f(\mathbf{r}) + v(\mathbf{r}) f(\mathbf{r}) = \lambda f(\mathbf{r}), \tag{2.62}$$

where r is less than the healing distance and

$$F_{\mathrm{J}}(\mathbf{R}) = \prod_{i<j} f(\mathbf{r}_{ij}). \tag{2.63}$$

Being the only spin dependent part of the trial wavefunction, the Slater determinant determines the anti-symmetry of the trial wavefunction, as required for a system of identical fermions, as well as the nodal surface of the trial wavefunction. A common choice is to calculate this using the non-interacting case for the fermions of interest, ie neutrons in pure neutron matter. This Slater determinant takes the form

$$D_{\mathrm{S}}(\mathbf{R}, S) = \frac{1}{N!}\epsilon_{i_1 \ldots i_N}\epsilon_{j_1 \ldots j_N}\langle \mathbf{r}_{i_1}, s_{i_1}|\phi_{j_1}\rangle \ldots \langle \mathbf{r}_{i_N}, s_{i_N}|\phi_{j_N}\rangle \tag{2.64}$$

where $\langle \mathbf{r}_i, s_i|\phi_i\rangle$ is the single-particle orbital ϕ for particle i. With this choice of the initial trial wavefunction, a set of Variational Monte Carlo calculations are done in order to reduce the variance in the energy. By doing this a better result for the trial wavefunction is obtained, which is then fed into the Auxiliary Field Diffusion Monte Carlo algorithm in order to obtain the final result.

Chapter 3

Fermi Liquid Theory and its Application to Infinite Nuclear Matter

3.1 The Free Fermi Gas

Having described the framework of Quantum Monte Carlo techniques needed to calculate accurate and precise energies, we will now motivate our choice of particle number in the simulations. We wish to calculate the energy per particle in the thermodynamic limit, but with each added particle in the simulated system, the calculations become intractable with existing hardware. Instead, there is a need to approximate using a finite number of particles, and reduce any inaccuracies resultant from not having the correct number of particles. These inaccuracies are dubbed "finite size effects".

For this, we examine the non-interacting problem of the Free Fermi Gas in three

spatial dimensions. First, we define our simulation cell to be cubic with a volume $V = L^3$, where L is the side length of the simulation cell. The cell can then be populated by a finite number of particles N, for which we can impose boundary conditions. For the purposes of simulating a large number of interacting particles, we impose the following periodic boundary conditions:

$$\Psi(x, y, z) = \Psi(x + lL, y + mL, z + nL) \tag{3.1}$$

onto our wavefunction $\Psi(x, y, z)$, with the integers l, m, n. Here, it is important to note that we are working with plane wave solutions to the Hamiltonian describing the system, which are non-normalizable in an infinite space, like that defined by the coordinates $\{x, y, z\}$. However, plane waves are able to be normalized in a finite space, or a phase space, where we choose the size of the box to be large relative to the interactions and particle size. This combined with the periodic boundary conditions allow an environment to simulate a large number of particles in a free space. This can be imagined as an array of identical cubic simulation cells that occupy all space. This is allowed, due the the translational invariance of the system. With this description, we may now examine the finite size effects alluded to above.

Since the calculations for the interacting system are limited in size, it is required that we consider finite-size effects. Let us consider the one-particle Hamiltonian of the free system in three dimensions

$$\hat{H} = -\frac{\hbar^2}{2m}\nabla^2, \tag{3.2}$$

for the time-independent Schrödinger equation:

$$-\frac{\hbar^2}{2m}\nabla^2\psi\left(\mathbf{r}\right)=E\psi\left(\mathbf{r}\right). \tag{3.3}$$

The plane wave solution to this system is given by

$$\psi\left(\mathbf{r}\right)=\frac{1}{\sqrt{V}}e^{i\mathbf{k}\cdot\mathbf{r}}, \tag{3.4}$$

where $\mathbf{k}$ is the wavevector defined by the integer quantum numbers n_x, n_y, n_z as

$$\frac{2\pi}{L}\left(n_x, n_y, n_z\right), \tag{3.5}$$

with the corresponding energy

$$E_{\mathbf{k}}=\frac{\hbar^2}{2m}\mathbf{k}^2. \tag{3.6}$$

For a Free Fermi Gas of fermions, the particles occupy the lowest available energy states. Since the energies are defined by $\mathbf{k}$, the ground state will be defined by the wavevector as a result. For a fermionic system of spin-1/2 particles, at most two fermions with opposite spin-projection can occupy the same wave vector $\mathbf{k}$, as governed by the Pauli Exclusion Principle. However, it is clear that there is a degeneracy in the various configurations, since there are multiple sets of quantum numbers n_x, n_y, n_z that can lead to the same energies. Because of this energetic degeneracy, the wavefunction is ambiguous whenever an occupied energy level is not completely filled because only a subset of degenerate states are occupied, and this subset is not guaranteed to be unique.

As is the case for fermionic systems, there exist closed shells, which correspond to energetically favoured states. The closed shell configurations for the Free Fermi Gas

occur at $N = 2, 14, 38, 54, 66, 114\ldots$ (Fig. 3.1). We are interested in the thermodynamic limit where the number of particles and volume of the system both approach infinity, with some well defined number density n, ie constant valued. For nuclear systems in particular, the thermodynamic limit of nucleons can be applied to the study of neutron stars.

Now because the thermodynamic limit is defined by $N \to \infty, V \to \infty$, we need a way to calculate the number density n, since simply dividing N by V at the thermodynamic yields an undefined quantity. However, the number density n is related to the magnitude of the maximal wavevector, or Fermi Wavevector, by

$$k_{\mathrm{F}} = \left(3\pi^2 n\right)^{1/3}. \tag{3.7}$$

This lends well to the energy per particle, given by

$$\epsilon_0 = \frac{3}{5}\frac{\hbar^2 k_{\mathrm{F}}^2}{2m} \tag{3.8}$$

$$\epsilon_0 = \frac{3}{5}E_{\mathrm{F}} \tag{3.9}$$

where E_{F} is the Fermi energy of the free particle system.

As above, the differences between an infinite system and a finite system result in finite size differences. These differences will of course go to zero in the thermodynamic limit. However, we can make use of closed-shell numbers in our simulations in order to curb these effects. Figure 3.1 plots the energy per particle against particle number for the Free Fermi Gas with no interactions. Of particular note, this plot is density-independent, meaning that these shell closures exist over a continuous spectrum of values for number density, which allows the study of various parameters as a function of n. From Fig. 3.1, there is a minimum in the finite size differences for 67 particles.

This demonstrates that for the nearest closed shell at 66 particles, we can choose this as a prime candidate for our studies. This will then be used as the basis in taking results to the thermodynamic limit.

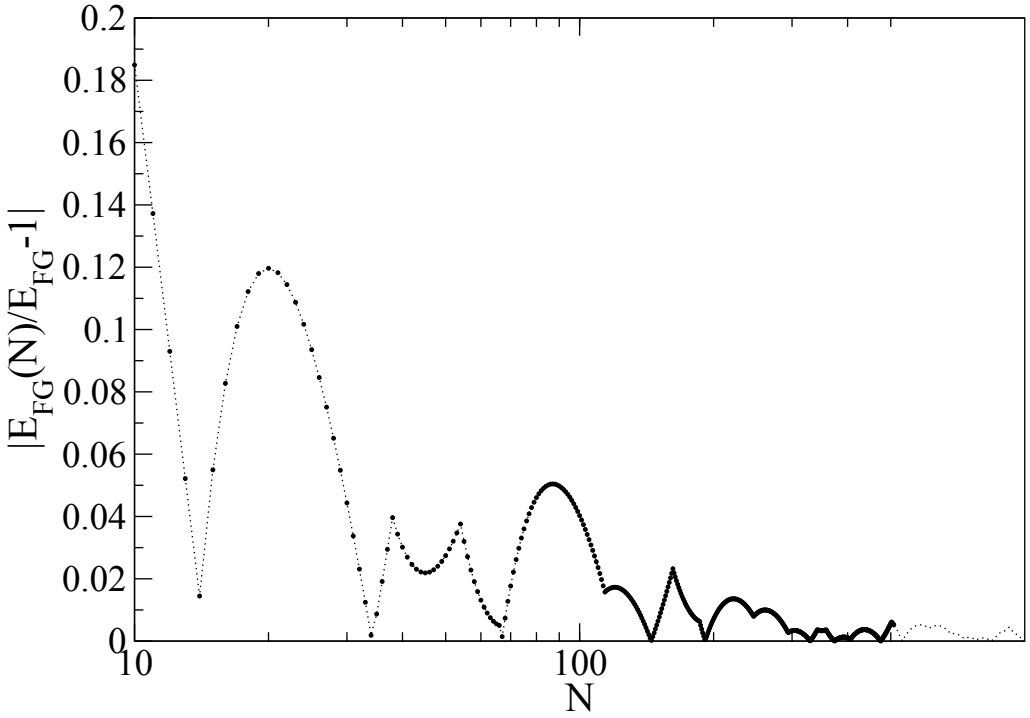

Figure 3.1: The free Fermi gas calculated using QMC demonstrates that there exist shell closures at certain particle numbers, resulting from finite-size effects. The finite size effects are plotted as a function of particle number, and we see that the minima exist at $N = 2, 14, 38, 54, 66, 114, \ldots$, which approximate the finite size effects vanishing in the thermodynamic limit.

For the non-interacting system, there exist constituents with particle and hole characteristics, with the free-particle dispersion relation ϵ_0. The total energy of a

system of N non-interacting fermions is given by

$$E = \sum_{\mathbf{p}} \frac{p^2}{2m} n(\mathbf{p}), \tag{3.10}$$

where $n_{\mathbf{p}}$ is the occupation of each of the states. The associated eigenstates are the anti-symmetrized combinations of the N single particle states of Eq. (3.4). The Fermi sphere is defined by the Fermi momentum, or wavevector given in Eq. (3.7).

If we add a single particle to the lowest available state at $p = p_{\mathrm{F}}$, we have for $T = 0$,

$$\mu = E_0(N+1) - E_0(N) = \frac{\partial E_0}{\partial N} = \frac{p_{\mathrm{F}}^2}{2m}. \tag{3.11}$$

Should the system be excited, some number of particles will be promoted across the Fermi Surface, and in their places will be corresponding holes below the Fermi Surface. These excitations are characterized by the difference in occupation number

$$\delta n(\mathbf{p}) = n(\mathbf{p}) - n_0(\mathbf{p}) = \begin{cases} \delta_{p,p'}, & \mathrm{for a particle if} p' > p_{\mathrm{F}} \\ -\delta_{p,p'}, & \text{for a hole if } \mathrm{p}' < \mathrm{p_F} \end{cases}. \tag{3.12}$$

Thus, the energy of the non-interacting system is completely characterized as a functional of the occupation

$$E - E_0 = \sum_{\mathbf{p}} \frac{\mathbf{p}^2}{2m} \delta n(\mathbf{p}). \tag{3.13}$$

Now in order to address the stability of the excitations, we consider the case of putting into contact our system with a particle bath. The free energy for $T = 0$ is

$$F - F_0 = \sum_{\mathbf{p}} \left(\frac{\mathbf{p}^2}{2m} - \mu \right) n(\mathbf{p}). \tag{3.14}$$

The free energy of a particle will correspond to an excitation outside the Fermi Surface, while for a hole will correspond to an excitation within the Fermi Surface. For both cases, the free energy for either at $p = p_{\mathrm{F}}$ is identically 0, because $\mu = p_{\mathrm{F}}/2m$, leading to the result of the Free energy of the system

$$\frac{p^2}{2m} - \mu > 0. \tag{3.15}$$

Since this quantity is always positive, the system is stable to excitations.

3.2 Fermi Liquid Theory

We are interested in studying excitations of interacting pure neutron matter. The machinery we have available to simulate this takes the form of Auxiliary Field Diffusion Monte Carlo (AFDMC). This framework takes in number density, the number of particles in the simulation box, their corresponding spin states, their corresponding **k**-state wavevector, and the interaction potential as inputs, and then outputs the energy per particle. With this we can begin to explore the excited states of interacting pure neutron matter through Landau Fermi Liquid Theory.

Fermi Liquid Theory by itself has success in describing the low-energy behaviour of interacting fermionic systems, like metals, ultracold atomic gases, and nuclear matter. The framework can be constructed several ways, from a many-body diagrammatic perspective or a phenomenological one. From the latter, there are some key assumptions to note:

1. Momentum and Spin are good quantum numbers to describe quasiparticle excitations.

2. Starting from the non-interacting system, one can adiabatically turn on the interactions between particles over some time t, resulting in the interacting system.

3. The excitations therein may be described as quasiparticles with lifetimes $\tau \gg t$.

As shown in the treatment for the Free Fermi Gas, excitations in this system are long-lived without the presence of an interaction, with the ground state specified by some ground state distribution function $n_0(\mathbf{p})$, where $\mathbf{p}$ represents the particle momenta.

In Landau Fermi Liquid Theory, it was proposed that interactions produce virtual particle-hole pairs, which means that the distribution functions above must change from $n_0(\mathbf{p})$ to $n_0(\mathbf{p})$. Further, it is assumed that the change in this distribution function is smooth, such that we can perform the adiabatic switching on of the interaction. However, if this adiabatic transition isn't smooth, and there exists a singularity, it would signal an instability of the ground state and should be viewed as a phase transition. If there are no phase transitions, or singularities, there should be a smooth connection between non-interacting and interacting states. As a result, the framework requires that the quantum numbers associated with the non-interacting states should also be good quantum numbers for the interacting states. For example, one-neutron (particle) state becomes a quasiparticle which carries the same charge (0) and spin (1/2) of the non-interacting neutron.

Now, the occupation of the interacting system can be written in terms of $n(\mathbf{p})$, and now for a stable system, it is required that $\delta n(\mathbf{p})$ is non-zero only for $|\mathbf{p}| \approx p_{\mathrm{F}}$, ie sufficiently close to the Fermi Surface. This implies that as the interaction turns

on and as as $n_0(p) \to n(p)$, that

$$n(p) = n_0(p) + \delta n(p) \tag{3.16}$$

where $n(p) \ll 1$, and similarly that

$$E = E_0 + \delta E, \tag{3.17}$$

where δE is the excitation energy. This excitation energy defines how much energy is required to add an excitation of a particular momentum state close to the Fermi Surface, and can be parameterized as

$$\delta E = \sum_p \epsilon \delta n(p) + \ldots \tag{3.18}$$

With this quantity, we can now take the quasiparticle energy to be

$$\epsilon(p) = \frac{\delta E}{\delta n(p)}. \tag{3.19}$$

The chemical potential of this interacting system may now be given by

$$\mu = E(N+1) - E(N), \tag{3.20}$$

and thus

$$\mu = \frac{\partial E}{\partial N} = \epsilon(p_{\mathrm{F}}). \tag{3.21}$$

In essence the low lying excited states with the addition of a quasiparticle are associated with a specified momentum, and thus $\mathbf{k}$. That is, $\epsilon(p)$ is not independent

of the existence of other quasiparticles, and thus, the energies can be parameterized as

$$E(\delta n) = \sum_{\mathbf{p}} \epsilon(p)\delta n(\mathbf{p}) + \frac{1}{2}\sum_{\mathbf{p},\mathbf{p}'} f(\mathbf{p},\mathbf{p}')\delta n(\mathbf{p})\delta n(\mathbf{p}') + \mathcal{O}(\delta n(\mathbf{p})^3), \tag{3.22}$$

where we have introduced the Landau interaction parameters $f(\mathbf{p},\mathbf{p}')$. Now, we can add spin state to the above quantities, correcting for any differences that arise from different spin combinations, which requires a slight change of notation. Further, in the machinery of our Quantum Monte Carlo techniques, the input parameters are more conveniently put in terms of $\mathbf{k}$, so we will rewrite the above as follows. The Landau energy functional is a parametrization of the ground state and excited state energies for our system :

$$E = E_0 + \sum_{\mathbf{k},\sigma} \mathcal{E}_\sigma(\mathbf{k})\,\delta\mathcal{N}_{\mathbf{k},\sigma} + \frac{1}{2}\sum_{(\mathbf{k},\sigma)\neq(\mathbf{k}',\sigma')} f_{\mathbf{k},\sigma,\mathbf{k}',\sigma'}\delta\mathcal{N}_{\mathbf{k},\sigma}\delta\mathcal{N}_{\mathbf{k}',\sigma'} + \mathcal{O}\left(\delta\mathcal{N}_{\mathbf{k}}^3\right), \tag{3.23}$$

where E_0 is the ground state energy, $\delta\mathcal{N}_{\mathbf{k},\sigma}$ is the change to the ground state quasiparticle occupation number for a wave-vector $\mathbf{k}$, spin σ, and $f_{\mathbf{k},\sigma,\mathbf{k}',\sigma'}$ is the Landau interaction function.

The energy of a single quasiparticle $\mathcal{E}_{\mathbf{k},\sigma}$ can be viewed formally as the functional derivative of Eq. (3.23),

$$\mathcal{E}_{\mathbf{k},\sigma} = \left(\frac{\delta E}{\delta\mathcal{N}_{\mathbf{k},\sigma}}\right)_{\mathcal{N}^{(0)}_{\mathbf{k},\sigma}}, \tag{3.24}$$

with respect to the quasiparticle distribution function evaluated at the ground-state. Now, if we just took the functional derivative without evaluating it at the ground state, we would get:

$$\tilde{\mathcal{E}}_{\mathbf{k},\sigma} = \frac{\delta E}{\delta\mathcal{N}_{\mathbf{k},\sigma}} = \mathcal{E}_{\mathbf{k},\sigma} + \sum_{\mathbf{k}',\sigma'} f_{\mathbf{k}',\sigma',\mathbf{k},\sigma}\delta\mathcal{N}_{\mathbf{k}',\sigma'}. \tag{3.25}$$

This derivative gives what is called the local quasiparticle energy, which can be interpreted as the energy of a single quasiparticle that has been modified by its interactions with other quasiparticles.

If we go one step further and take another functional derivative with respect to the quasiparticle distribution, we can relate the local quasiparticle energy to the Landau interaction function as

$$f_{\mathbf{k},\sigma,\mathbf{k}',\sigma'} = \frac{\delta^2 E}{\delta \mathcal{N}_{\mathbf{k},\sigma} \delta \mathcal{N}_{\mathbf{k}',\sigma'}} = \frac{\delta \tilde{\mathcal{E}}_{\mathbf{k},\sigma}}{\delta \mathcal{N}_{\mathbf{k}',\sigma'}}. \tag{3.26}$$

From here onwards, we will denote $f_{\mathbf{k},\sigma,\mathbf{k}',\sigma'}$ as $f_{\sigma,\sigma'}(\theta)$, where θ is the angle between the wave-vectors $\mathbf{k}$ and $\mathbf{k}'$. This change in notation also reflects the lack of dependence on the individual vectors, and the dependence on the angle between the vectors. Using this information derived from the rotational invariance of the system, we recognize that we can use an expansion of the form

$$f_{\mathbf{k},\mathbf{k}'} = \sum_{l=0}^{\infty} f_l P_l(\cos\theta), \tag{3.27}$$

and thus for the 3-dimensional case, the expression for the l^{th} Fermi liquid parameters is

$$F_l^{\text{s,a}} = \frac{VN^*}{8\pi} \int P_l(\cos\theta) \left[f_{\uparrow\uparrow}(\theta) \pm f_{\uparrow\downarrow}(\theta) \right] \mathrm{d}\Omega, \tag{3.28}$$

where we defined these over the angular momentum channels. Once again, θ is the angle between the vectors $\mathbf{k}$ and $\mathbf{k}'$, P_l is the l^{th} Legendre Polynomial, V is the volume of the simulation cell, and $N^*(0)$ is the density of quasiparticle states per unit volume at the Fermi level. Here, the s stands for symmetric (the sum of the interaction functions) and a stands for asymmetric (the difference of the interaction functions).

The $*$ in $N^*(0)$ is to show that this differs from the non-interacting case, by replacing the mass m with the effective mass m^* in the expression for density of quasiparticle states per unit volume at the Fermi level as:

$$N^* = \frac{m^*}{m}N = \frac{m^*}{m}\frac{m}{2\pi^2}\frac{k_F}{\hbar^2} = \frac{m^*}{2\pi^2}\frac{(3\pi^2 n)^{1/3}}{\hbar^2}, \tag{3.29}$$

where n is the number density. Plugging Eq. (3.29) into Eq. (3.28), we can recast the expression for the Fermi liquid parameter to an expression for the Fermi liquid parameter divided by the effective mass as

$$\frac{F_l^{\mathrm{s,a}}}{m^*} = \frac{V}{8\pi^{4/3}\hbar^2}(3n)^{1/3}\int_0^\pi \left[f_{\uparrow\uparrow}(\theta) \pm f_{\uparrow\downarrow}(\theta)\right] P_l(\cos\theta)\sin\theta \mathrm{d}\theta. \tag{3.30}$$

This form is going to be useful when calculating quantities like the ratio of the effective mass to the mass, compressibility, spin susceptibility, and g-factor.

3.3 Extending to the Thermodynamic Limit

First, we may evaluate the Landau interaction functions at a discrete set of angles $\{\theta_i\}$ as

$$f_{\sigma,\sigma'}(\theta_i) = -\left[E_{\sigma,\sigma'}(\mathbf{k}_i, \mathbf{k}_i') + E_0 - E_{+,\sigma}(\mathbf{k}_i) - E_{-,\sigma'}(\mathbf{k}_i')\right] \tag{3.31}$$

where E_0 is the ground state energy – that is the energy for N interacting neutrons – and $E_{\sigma,\sigma'}(\mathbf{k}_i, \mathbf{k}_i')$ is the energy where a neutron has been promoted from $\mathbf{k}_i'$ to $\mathbf{k}_i$. Explicitly, the latter is the energy for N interacting neutrons, where a neutron with $(\mathbf{k}_i', \sigma')$ is removed, and in its place a neutron with $(\mathbf{k}_i, \sigma)$ is added. $E_{+,\sigma}(\mathbf{k}_i)$ is the energy where a neutron has been added to the state with $(\mathbf{k}_i, \sigma)$ – the energy for $N+1$ interacting neutrons where the added neutron occupies $(\mathbf{k}_i, \sigma)$ – and $E_{-,\sigma'}(\mathbf{k}_i')$

is the energy where a neutron has been removed from the state $(\mathbf{k}_i', \sigma')$ – the energy for $N-1$ neutrons where the removed neutron had occupied the state $(\mathbf{k}_i', \sigma')$.

Now it is clear that Eq. (3.31) is for finite N, rather than for an infinite number of particles in an infinite volume, corresponding to the thermodynamic limit. As a result, this means that we should expect some finite size effects, similar to what was described in the previous section.

Let us consider what would happen in trying to take $f_{\sigma,\sigma'}(\theta_i)$ to the thermodynamic limit, which we will denote as follows $f^{\mathrm{TL}}_{\sigma,\sigma'}(\theta_i)$. As discussed by Buraczynski, Ismail, and Gezerlis [69], about some N for which a particle has been added to a state $\mathbf{k}$, the energy difference taken at the thermodynamic limit is given by

$$\begin{aligned}
\Delta E_N^{(\mathrm{TL})}(\mathbf{k}) &= \Delta E(\mathbf{k}) - \Delta T(\mathbf{k}) + \frac{\hbar^2}{2m} k_{\mathrm{TL}}^2 && (3.32)\\
\Delta E(\mathbf{k}) &= E_{N+1}(\mathbf{k}) - E_N + \frac{2}{5}\xi E_{\mathrm{F}} && (3.33)\\
\Delta T(\mathbf{k}) &= T_{N+1}(\mathbf{k}) - T_N + \frac{2}{5} E_{\mathrm{F}} && (3.34)\\
k_{\mathrm{TL}}^2 &= k^2 - k_{\mathrm{F},N}^2 + k_{\mathrm{F}}^2. && (3.35)
\end{aligned}$$

To apply this to our results, we can recast Eq. (3.31) as follows:

$$\begin{aligned}
f_{\sigma,\sigma'}(\theta_i) &= -\left[E_{\sigma,\sigma'}(\mathbf{k}_i, \mathbf{k}_i') + E_0 - E_{+,\sigma}(\mathbf{k}_i) - E_{-,\sigma'}(\mathbf{k}_i')\right]\\
f_{\sigma,\sigma'}(\theta_i) &= -\left[\left(E_{\sigma,\sigma'}(\mathbf{k}_i, \mathbf{k}_i') - E_{-,\sigma'}(\mathbf{k}_i')\right) - \left(E_{+,\sigma}(\mathbf{k}_i) - E_0\right)\right]\\
f_{\sigma,\sigma'}(\theta_i) &= -\left[\Delta E_{\sigma,\sigma',N-1}(\mathbf{k}_i, \mathbf{k}_i') - \Delta E_{\sigma,N}(\mathbf{k}_i)\right]\\
\implies f^{\mathrm{TL}}_{\sigma,\sigma'}(\theta_i) &= -\left[\Delta E^{(\mathrm{TL})}_{\sigma,\sigma',N-1}(\mathbf{k}_i, \mathbf{k}_i') - \Delta E^{(\mathrm{TL})}_{\sigma,N}(\mathbf{k})\right]\\
f^{\mathrm{TL}}_{\sigma,\sigma'}(\theta_i) &= -\left[\left(E_{\sigma,\sigma'}(\mathbf{k}_i, \mathbf{k}_i') - E_{-,\sigma'}(\mathbf{k}_i') - T_N(\mathbf{k}_i, \mathbf{k}_i') + T_{N-1}(\mathbf{k}_i') + \frac{\hbar^2}{2m}(\mathbf{k}_{i,N}^2 - k_{\mathrm{F},N-1}^2)\right)\right.\\
&\qquad \left. - \left(E_{+,\sigma}(\mathbf{k}_i) - E_0 - T_{N+1}(\mathbf{k}_i) + T_N + \frac{\hbar^2}{2m}(\mathbf{k}_{i,N+1}^2 - k_{\mathrm{F},N}^2)\right)\right]
\end{aligned}$$

Note that in the above, the $E_{\rm F}$ terms were canceled right away. We now rearrange the terms further to arrive at a more digestible result:

$$\begin{aligned} f^{\rm TL}_{\sigma,\sigma'}(\theta_i) &= f_{\sigma,\sigma'}(\theta_i) - -\left[\left(T_N(\mathbf{k}_i,\mathbf{k}'_i) - T_{N-1}(\mathbf{k}'_i)\right) - \left(T_{N+1}(\mathbf{k}_i) - T_N\right)\right] + \\ &\quad \frac{\hbar^2}{2m}\left(\left(k^2_{F,N-1} - \mathbf{k}^2_{i,N}\right) - \left(k^2_{F,N} - \mathbf{k}^2_{i,N+1}\right)\right) \\ f^{\rm TL}_{\sigma,\sigma'}(\theta_i) &= f_{\sigma,\sigma'}(\theta_i) - f^T(\theta_i) + \frac{\hbar^2}{2m}\left(\left(\mathbf{k}^2_{i,N+1} - k^2_{F,N}\right) - \left(\mathbf{k}^2_{i,N} - k^2_{F,N-1}\right)\right) \end{aligned} \quad (3.36)$$

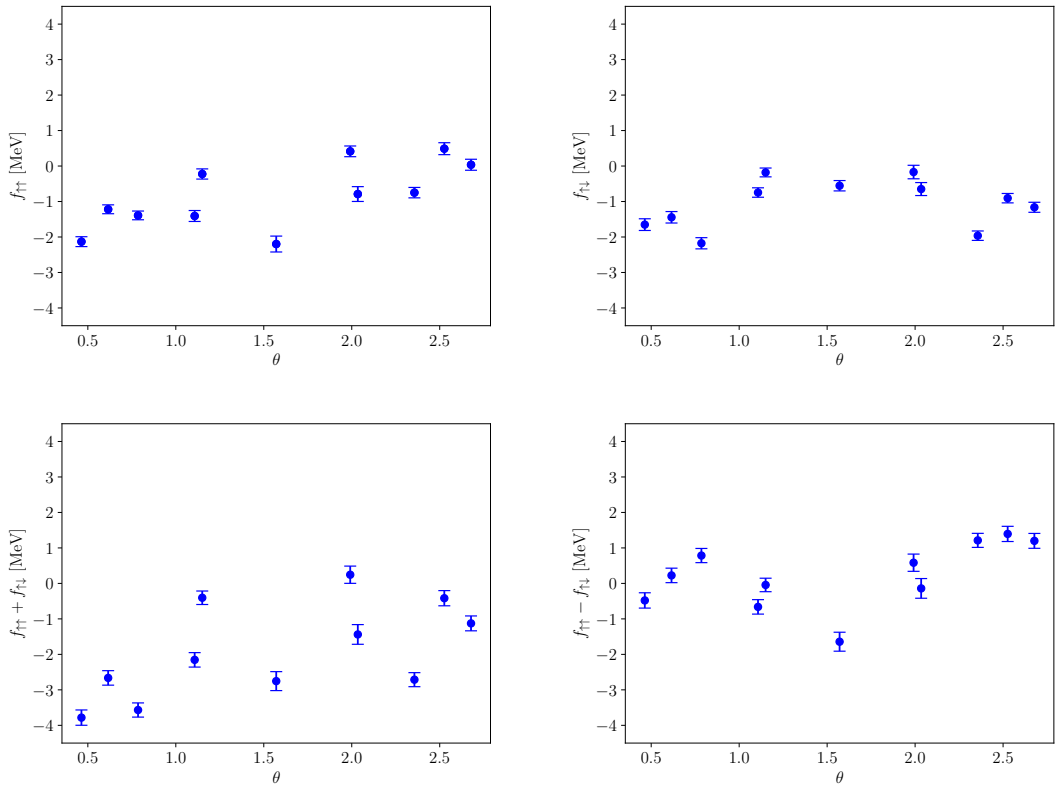

Figure 3.2: On the upper left is the Landau interaction function for the case of a spin up particle being promoted to a excited spin up state, on the upper right is the Landau interaction function for the case of a spin down particle being promoted to a excited spin up state. In the bottom left is the sum of the Landau interaction functions, and in the bottom right is the difference of the Landau interaction functions. These plots were all done for the finite case of $N = 66$ neutrons, using Auxiliary Field Diffusion Monte Carlo. The error bars on this plot are statistical errors that result from the block averaging of AFDMC energies.

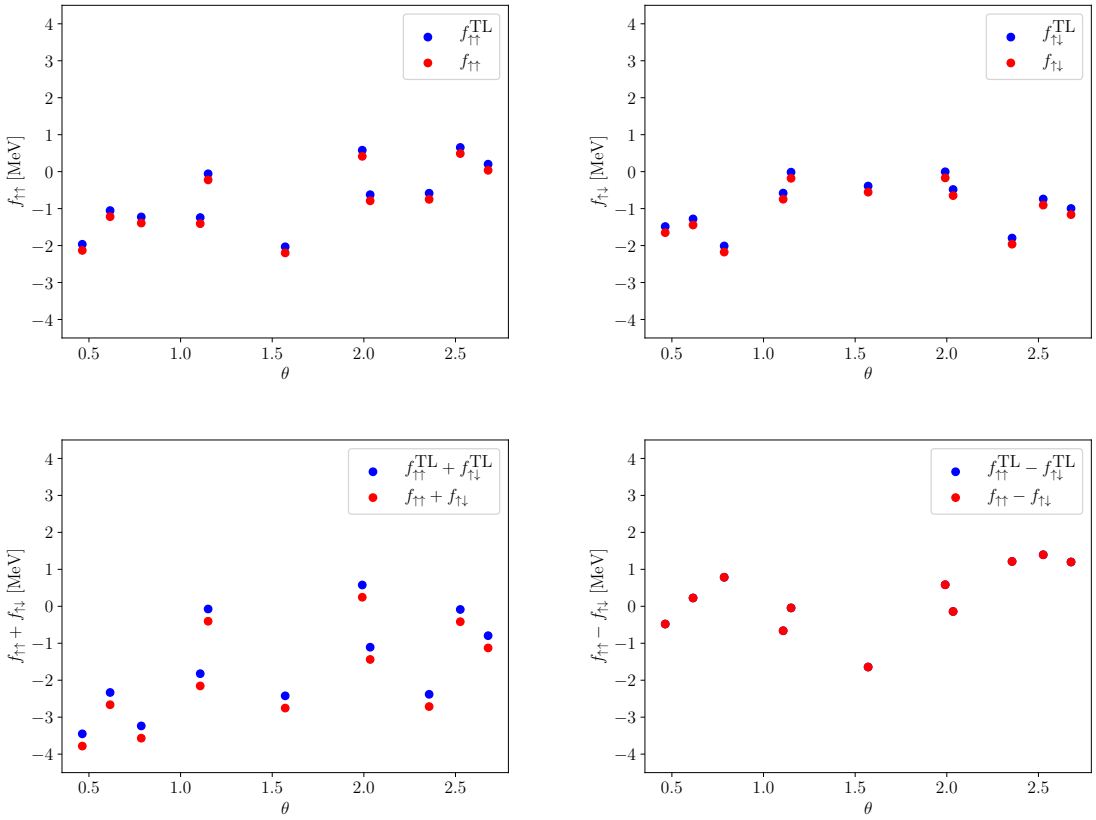

Figure 3.3: On the upper left is the Landau interaction function for the case of a spin up particle being promoted to a excited spin up state, on the upper right is the Landau interaction function for the case of a spin down particle being promoted to a excited spin up state. In the bottom left is the sum of the Landau interaction functions, and in the bottom right is the difference of the Landau interaction functions. Red circles correspond to the finite case, and blue circles to the thermodynamic limit. Errors are left off this plot for clarity in comparing the finite case to the extrapolation to the thermodynamic limit.

Thus, the Landau interaction function at the thermodynamic limit, $f_{\sigma,\sigma'}^{\mathrm{TL}}(\theta_i)$, is the Landau interaction function for the finite case, subtracting off the non-interacting kinetic energies for the finite case (grouped into what is denoted as $f^T(\theta_i)$) and adding a term with the difference of the quadrature differences of relevant $\mathbf{k}$ vectors. The $\mathbf{k}_{i,N}$ corresponds to the excited state which the quasiparticle occupies with a simulation volume for N particles, and $k_{F,N-1}$ is the highest occupied k state without the excitation with a simulation volume for N particles. Now, the second term, $f^T(\theta_i)$

in Eq. (3.36), when explicitly written has the form of Eq. (3.31). Thus we think of it as a sort of finite-size-effect Landau interaction function, where the contribution comes from the difference in the kinetic energies. These kinetic energies don't simply cancel out, because of the different simulation volumes for the different particle numbers N (as the number density n was kept constant). This is why the notation $f^T(\theta_i)$ is used, where the T is there to represent that it only involves the kinetic energies of the free particles.

Table 3.1: Fermi liquid parameters calculated for $n = 0.06$ fm^{-3} and $N = 66$ neutrons interacting through the av8'+uix potential.

	Trapezoid	Right Riemann	Left Riemann
F_0^s	$(-1.32 \pm 0.07) \times 10^{-3}$	$(-1.3 \pm 0.1) \times 10^{-3}$	$(-1.4 \pm 0.1) \times 10^{-3}$
F_0^a	$(-8 \pm 6) \times 10^{-5}$	$(-0.2 \pm 1) \times 10^{-4}$	$(-1 \pm 1) \times 10^{-4}$
F_1^s	$(-2.0 \pm 0.8) \times 10^{-4}$	$(-1 \pm 1) \times 10^{-4}$	$(-3 \pm 2) \times 10^{-4}$
F_1^a	$(-1.2 \pm 0.8) \times 10^{-4}$	$(-2 \pm 2) \times 10^{-4}$	$(-0.4 \pm 2) \times 10^{-4}$
F_2^s	$(6 \pm 3) \times 10^{-5}$	$(9 \pm 6) \times 10^{-5}$	$(3 \pm 6) \times 10^{-5}$
F_2^a	$(2 \pm 2) \times 10^{-4}$	$(2.4 \pm 0.3) \times 10^{-4}$	$(2.1 \pm 0.3) \times 10^{-4}$

Now, we compute the Landau interaction functions for $N = 66$ neutrons at a number density of $n = 0.06$ fm^{-3}, using Auxiliary Field Diffusion Monte Carlo with an av8'+uix interaction. This interaction encapsulates both nucleon–nucleon (NN) and nucleon–nucleon–nucleon (NNN) interactions.

We choose $\{\mathbf{n}'\} = \{(-2,0,0),\ (0,-2,0),\ (0,0,-2),\ (2,0,0),\ (0,2,0)\}$ and $\{\mathbf{n}\} = \{(-2,-1,0),(-2,-1,-1),(-2,-2,0),(-3,0,0)\}$, which gives a set of discrete θ and associated values of $f_{\sigma,\sigma'}$. This set of $\mathbf{n}'$ are chosen, because they are the correspond to the highest occupied quantum numbers for $N = 66$ particles. This set of $\mathbf{n}'$ are chosen, because they correspond to the quantum numbers used to calculate the results for effective mass in the later sections, thus allowing for direct comparison between methods. Further, it has been demonstrated for these parameters that quasiparticles occupying these states follow a quadratic dispersion relation, as they are close to the

Fermi level as expected.

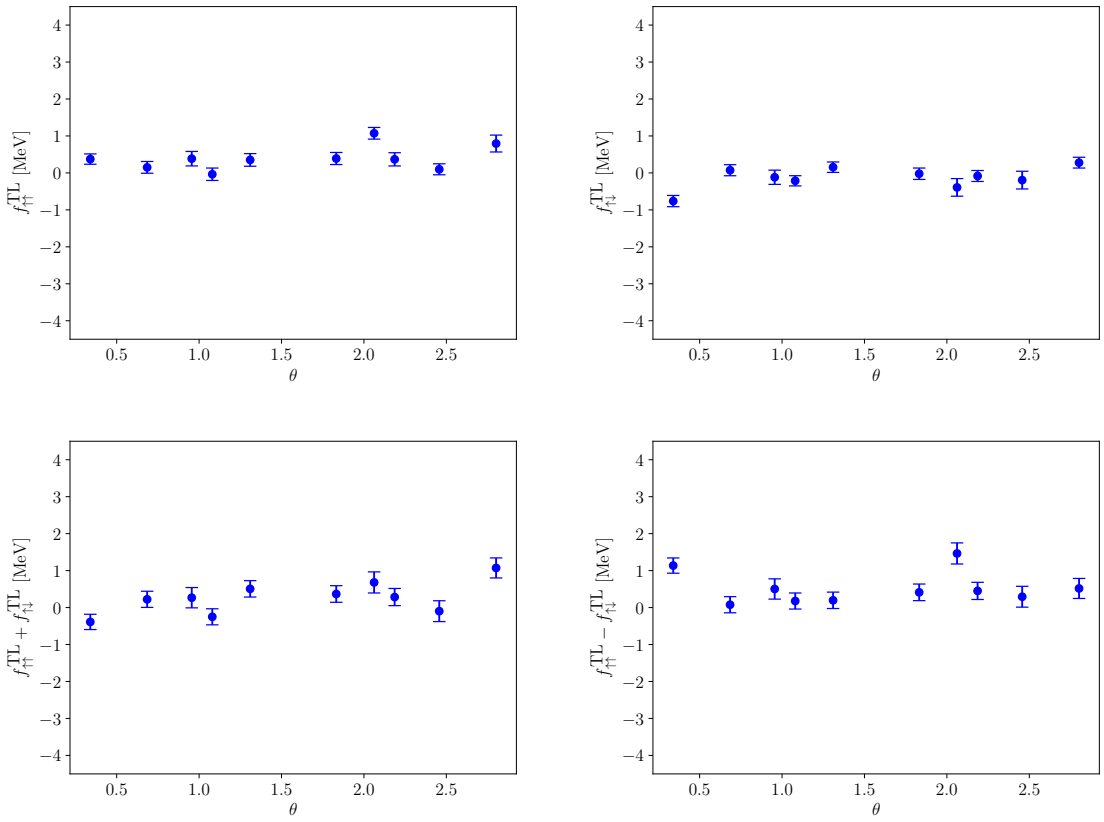

Figure 3.4: On the upper left is the Landau interaction function for the case of a spin up particle being promoted to a excited spin up state, on the upper right is the Landau interaction function for the case of a spin down particle being promoted to a excited spin up state. In the bottom left is the sum of the Landau interaction functions, and in the bottom right is the difference of the Landau interaction functions. These plots were all done for the finite case of $N = 54$ neutrons, using Auxiliary Field Diffusion Monte Carlo, which were then extrapolated to the thermodynamic limit. The error bars on this plot are statistical errors that result from the block averaging of AFDMC energies. In contrast to the $N = 66$ case, the data points are smaller in deviation.

Prior to the AFDMC simulations, we run a Variational Monte Carlo simulations to optimize the wavefunction. Once again, we stress that the accuracy of the wavefunction determines the accuracy of the results in the AFDMC calculations, and by using VMC to first calculate a more accurate wavefunction, we are able to achieve more accurate results through AFDMC.

In Fig. 3.2 we plot the results of the Landau interaction functions for 66 neutrons. Here, the errors are statistical errors that result from the averaging of the energies resultant from the AFDMC calculations, which propagate through Eq. (3.31). The averaging is done through block averaging and sampling, in order to reduce correlations between successive energies in the AFDMC calculations.

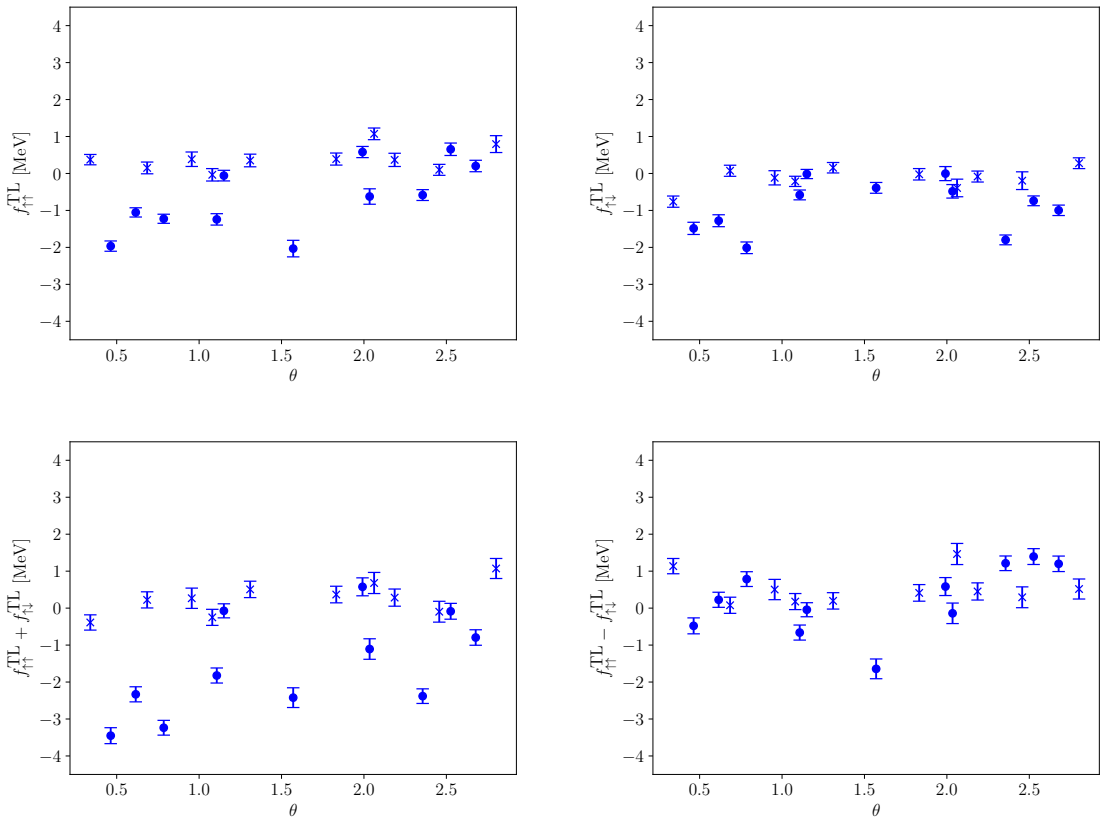

Figure 3.5: On the upper left is the Landau interaction function for the case of a spin up particle being promoted to a excited spin up state, on the upper right is the Landau interaction function for the case of a spin down particle being promoted to a excited spin up state. In the bottom left is the sum of the Landau interaction functions, and in the bottom right is the difference of the Landau interaction functions. In each of these plots the circles correspond to results extrapolated from the $N = 66$ case, while the crosses correspond to the results extrapolated from the $N = 54$ case. These were all calculated from Auxiliary Field Diffusion Monte Carlo energies, which were then extrapolated to the thermodynamic limit. The error bars on this plot are statistical errors that result from the block averaging of AFDMC energies.

These functions have few data points, because the particle excitations are required

to be close to the Fermi surface, meaning that we are limited to only a few configurations of the quantum numbers n_x, n_y, n_z for the excited particle. Further, we explored by running more simulations with different $\{\mathbf{n}\}$ and $\{\mathbf{n}'\}$ that have the same set of angles, to see if they yield different energy differences and subsequent Landau interaction functions. They did not produce differences outside of error, verifying the dependence only on angle between the wavevectors as opposed to vector quantities.

Note that because we are limited to a small number of data points, that we expect the error from the numerical integration to be large. It is for this reason that multiple integration methods will be compared used and compared. Specifically, we will use left Riemann sums, right Riemann sums, and the trapezoid rule to calculate the Fermi liquid parameters, and tabulate them side-by-side to compare (Tab. 3.1). The results show little difference, and as such, we choose the trapezoid rule for numerical integration between the discrete data points for the Landau interaction functions.

This can be improved upon by exciting particles about other shell closures, adding more data points, which we will address after first examining the extrapolation to the thermodynamic limit.

It is clear from Fig. 3.3, that the finite-size corrections for the above parameters serve to increase the value of the Landau interaction functions. Further, the finite-size corrections don't change any trend in $f_{\sigma,\sigma'}(\theta)$ between the finite case and the extrapolation to the thermodynamic limit.

Next, we can look at the closest shell closure motivated by Fig. 3.1 about $N = 54$ neutrons. Around this shell closure, there are 10 appropriate angles that can be chosen, resulting from quantum numbers adequately close to the Fermi level. The resulting Landau interaction function is plotted in Fig. 3.4 for which each calculated value was extrapolated to the thermodynamic limit.

Of particular note here is that the function has a significantly smaller variance than for the case of the Landau interaction function calculated from the $N = 66$ values. This is partially explained by the nature of the strong force. It is non-perturbative, and it is expected that about shell closures for greater particle numbers that the energy associated with (quasi)particle excitations is more pronounced. This results in greater differences in energies, and thus a greater variance in the Landau interaction function.

That being said, with these added results it is now possible to plot a greater number of data points, as in Fig. 3.5. In this plot, we can read off the plots that the Landau functions calculated from $N = 66$ particle energies tend to have slightly lower values than for those calculated from $N = 54$ energies. However, the deviation is not significant enough to imply a systematic cause resultant from the choice of quantum numbers. Further, since it was tested that the values of the Landau interaction functions were only dependent on the angle, and not the quantum numbers chosen, we find that the choice of shell closure was not significant for quantum numbers that resulted in the same angle. Thus we further rule out any potentially systematic error in these calculations. It was found that with the addition of the new data points that the Fermi Liquid parameters reported in Tab. 3.1 did not change within the reported error. However, for the calculation of observables in the following subsections, we will use the values for the Fermi liquid parameters found from the entire parameter set, rather than the values from just the $N = 66$ case. The errors will propagate through accordingly.

3.3.1 Effective Mass

The effective mass, m^* of a particle is the apparent mass of a particle interacting within some medium. In principle, this effective mass is a result of the interactions and forces within a material, and as such is often reported as a bulk property for a material. Often this quantity is found through a dispersion relation, relating the energy of the particle to the momentum in k space. As such, the effective mass can correspond to quasiparticles and excitations, rather than just particles with a well-defined rest mass, like a nucleon or an electron.

Let us consider the non-interacting case first. Non-interacting particles follow the dispersion relation:

$$E = \frac{\hbar^2}{2m}k^2. \tag{3.37}$$

From this relation, it is clear that if the magnitude of the wavevector and corresponding energy is known, that the mass may be found from the slope of the function. This linear relation is a simple one derived from the free-particle case, however this idea can be extended to the interacting case.

For a general system the effective mass is defined by the approximation:

$$E \approx \frac{\hbar^2}{2m^*}k^2 \tag{3.38}$$

It is typically computed through the first or second derivative of energy with respect to wave-vector. In the case of finite particles, we are restricted in the allowed k values and must make do with a quadratic fit to extract m^*. Furthermore, we study effective mass at the Fermi surface where our simulations can probe various k values above the surface. We cannot probe already occupied levels due to the Pauli

exclusion principle.

We introduce the details of our method in the context of the free-Fermi gas where an "effective mass" arises due to the way we have chosen to handle finite size effects. Consider the ground-state of N particles of free fermions at some density n. Denote the energy of the system as $F_n(N)$. Now consider adding a particle with momentum vector k while keeping density constant. Denote the energy as $F_n^k(N+1)$. We are interested in the single-particle energy E_k^{Free} of the $N+1^{th}$ particle. In the thermodynamic limit:

$$\begin{aligned} F_n(N+1) - F_n(N) &= \frac{3}{5}E_F \\ F_n^k(N+1) - F_n(N+1) &= E_k^{Free} - E_F \end{aligned} \tag{3.39}$$

Adding the above expressions together yields:

$$E_k^{Free} = \Delta F_n^k(N) + \frac{2}{5}E_F \tag{3.40}$$

where $\Delta F_n^k(N) = F_n^k(N+1) - F_n(N)$. Computing an effective mass from this equation yields the rest mass in the thermodynamic limit. At finite N the effective mass has finite size effects because Eq. 3.40 was derived in the TL.

We have computed the effective mass for homogeneous neutron matter. Unlike the free-Fermi effective mass, we are very limited with system size. We calculate energies for smaller particle numbers and extrapolate/extend to the TL with a particular prescription. We define $I_n^k(N+1)$ and $I_n(N)$ for the interacting energies analogously to their non-interacting counterparts $F_n^k(N+1)$ and $F_n(N)$. We have:

$$E_k^{Int} = \Delta I_n^k(N) + \frac{2}{5}\xi E_F \tag{3.41}$$

where $\frac{3}{5}\xi E_F$ is the TL energy per particle. Fitting E_k^{Int} versus k to $E_k^{Int} = \frac{\hbar^2}{2m^*}k^2$ yields the unextended effective mass, albeit suffering from the TL derived $\frac{2}{5}\xi E_F$ term. We extrapolate to the TL using:

$$\Delta I_n^{k_\infty}(\infty) = \Delta I_n^k(N) - \Delta F_n^k(N) + \Delta F_n^{k_\infty}(\infty) \tag{3.42}$$

where $\Delta F_n^{k_\infty}(\infty)$ is the fixed density energy difference of adding a single particle at k_∞ to the free-Fermi gas at the TL. k_∞ satisfies:

$$k^2 - k_g^2 = k_\infty^2 - k_F^2 \tag{3.43}$$

and k_g is the maximum occupied wave-vector of the N particle ground-state (i.e. a Fermi surface for the finite system). This is to say that we fix the energy difference between the Fermi surface and the energy level of the excited particle. We have that:

$$\Delta F_n^{k_\infty}(\infty) = \frac{\hbar^2}{2m}k_\infty^2 - \frac{2}{5}E_F \tag{3.44}$$

which follows from adding together the TL expressions:

$$F_n(N+1) - F_n(N) = \frac{3}{5}E_F \quad \text{and} \quad \mathrm{F_n^{k_\infty}(N+1) - F_n(N+1) = \frac{\hbar^2}{2m}k_\infty^2 - E_F}$$

Thus we have:

$$\begin{aligned} E_{k_\infty}^{Int} &= \Delta I_n^{k_\infty}(\infty) + \frac{2}{5}\xi E_F \\ &= \Delta I_n^k(N) - \Delta F_n^k(N) + \frac{\hbar^2}{2m}k_\infty^2 - \frac{2}{5}E_F + \frac{2}{5}\xi E_F \\ &= E_k^{Int} - E_k^{Free} + \frac{\hbar^2}{2m}k_\infty^2 \end{aligned} \tag{3.45}$$

Note that both the finite N single-particle energies E_k^{Int} and E_k^{Free} contain finite size effects.

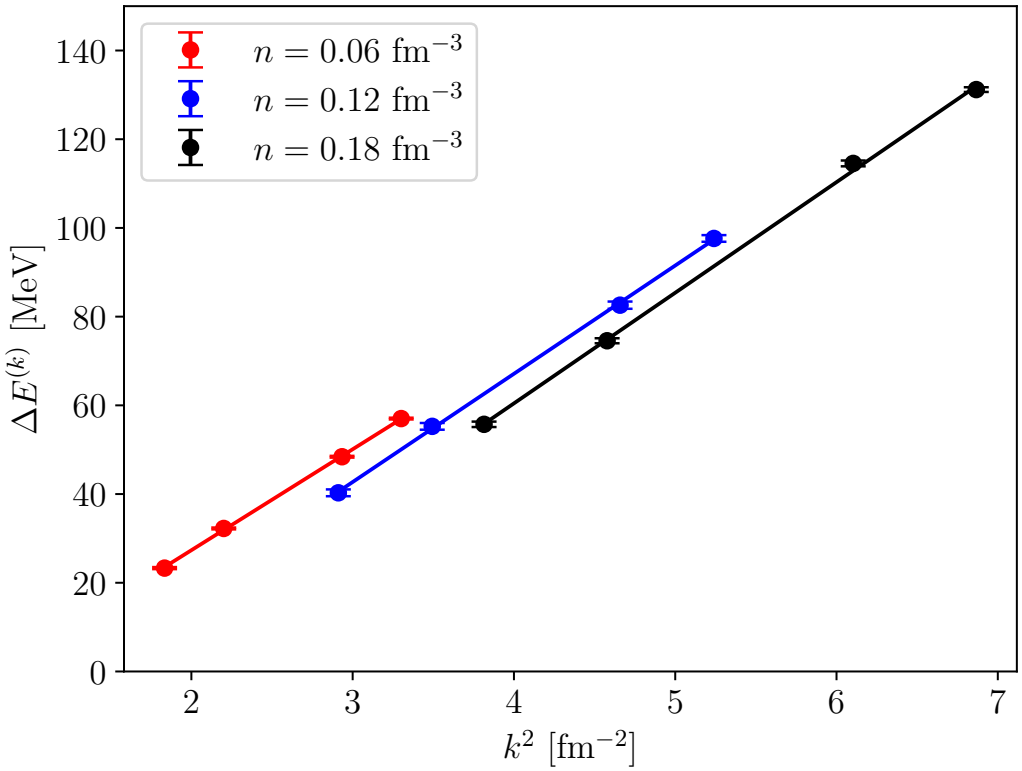

Figure 3.6: Plotted here is the quasiparticle energy as a function of the square of the wave-vector for the number densities $n = 0.06, 0.12, 0.18$ fm^{-3}, neutrons interacting through a av8'+uix potential at the thermodynamic limit. Note the linear trend of each line and how it demonstrates the validity of the dispersion relation in Eq. (3.47).

In this fashion, we are able to extract effective mass directly from the energy band ΔE^k for the excited quasiparticle from the following relations:

$$\Delta E^k = E^k_{N+1} - E_N + \frac{2}{5}\xi E_F \tag{3.46}$$

$$\Delta E^k = \frac{\hbar^2}{2m^*}k^2. \tag{3.47}$$

In Eq. (3.46), $E^k_{\mathrm{N+1}}$ is the energy for N+1 particles where the N+1$^{\mathrm{th}}$ particle is the excited state corresponding to state k, and ξ is the Bertsch parameter, which is

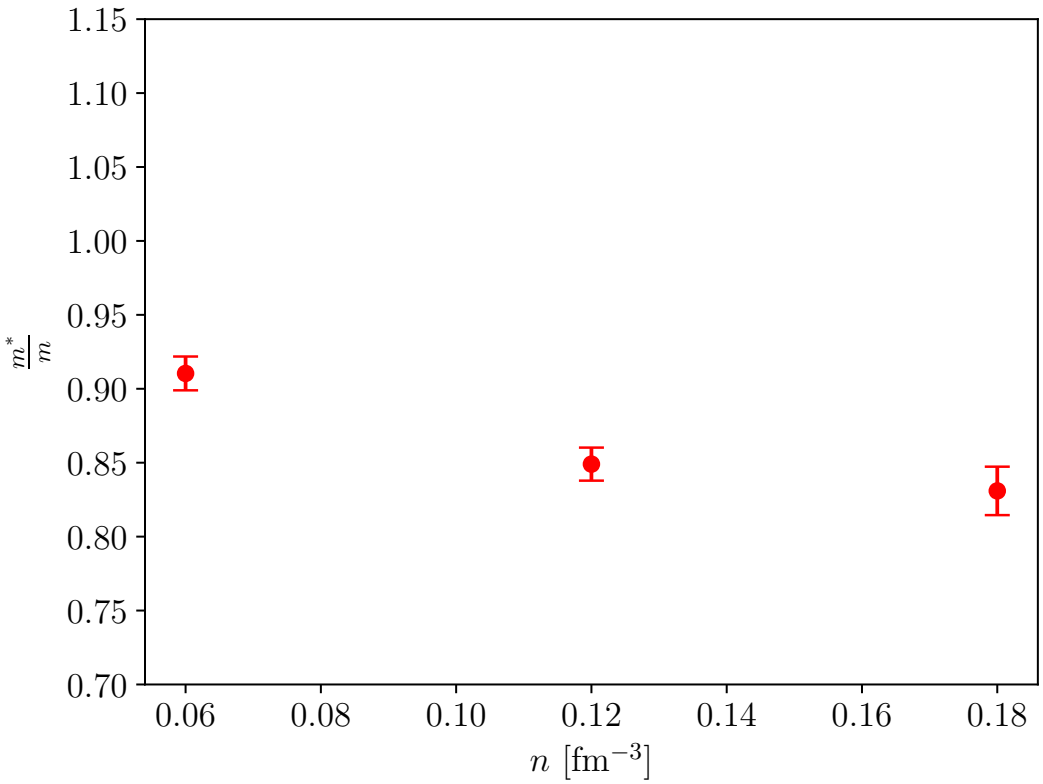

Figure 3.7: Plotted here is the ratio of effective mass to the rest mass of the neutron. Here it is plotted as a function of number density for neutrons interacting through a av8'+uix potential. Here, the effective masses were calculated from the slope of the dispersion relation shown in Fig. 3.6, using Eq. (3.47).

defined by $\bar{E}_\infty = (3/5)\xi E_F$, relating the energy per particle for an infinite amount of particles $\bar{E}_\infty$ to the Fermi energy E_F. By Eq. (3.47), the effective mass can be extracted as the slope of $\bar{E}_\infty$ as a function of k^2, as shown in Fig. 3.6 and Fig. 3.7 for several densities interacting with the av8'+uix potentials. Interestingly, due to the formulation described for treatment at the thermodynamic limit, the slope remains the same, meaning that the effective mass found at the finite case is the same for at the thermodynamic limit.

Now, to derive the effective mass in the framework of Fermi Liquid Theory, let us first consider a Galilean invariant system. For a transformation that involves a speed

$\vec{v}$, we have

$$E' = E - \vec{P}\cdot\vec{v} + \frac{1}{2}M\vec{v}^2 \tag{3.48}$$

$$\vec{P}' = \vec{P} - M\vec{v}, \tag{3.49}$$

where the capitalized variables correspond to the total energy E, momentum $\vec{P}$, and mass M, in the lab frame. If a quasiparticle of momentum $\vec{p}$ in the lab frame is added of some mass m, the moving frame momentum and energy increase by

$$\vec{p} - m\vec{v} \tag{3.50}$$

$$\epsilon_\sigma(\vec{p}) - \vec{p}\cdot\vec{v} + \frac{1}{2}m\vec{v}^2, \tag{3.51}$$

where we have $\epsilon_\sigma(\vec{p})$ being the energy increase of the system in the lab frame due to the addition of the quasiparticle.

Next, we can write the transformation as

$$\epsilon'_\sigma(\vec{p} - m\vec{v}) = \epsilon'_\sigma(\vec{p}) - \vec{p}\cdot\vec{v} + \frac{1}{2}m\vec{v}^2 \tag{3.52}$$

$$\implies \epsilon'_\sigma(\vec{p}) = \epsilon_\sigma(\vec{p}' + m\vec{v}) - \vec{p}\cdot\vec{v} - \frac{1}{2}m\vec{v}^2 \tag{3.53}$$

consistent with the Galilean invariance of the system. Applying a Taylor expansion in $\vec{v}$ and making use of the definition of effective mass, we have

$$\epsilon'_\sigma(\vec{p} - m\vec{v}) = \epsilon_\sigma(\vec{p}) + \left(\frac{m - m^*}{m}\right)\vec{p}\cdot\vec{v} + \ldots \tag{3.54}$$

Now, we can apply the Galilean transformation to the occupation numbers as

$$n'\left(\vec{p}\right) = n^0\left(\vec{p} + m\vec{v}\right) + m\vec{v}\cdot\partial_{\vec{p}} n^0\left(\vec{p}\right) + \ldots, \tag{3.55}$$

where we note that for the moving frame, the ground state (denoted by the ^{0} superscript) acts like a Fermi surface centered about $\vec{p} = -m\vec{v}$. Thus, the quasiparticle energy in the moving frame is

$$\epsilon'_\sigma\left(\vec{p}\right) = \epsilon_{\sigma,\vec{p}}\left(n'\left(\vec{p}'\right)\right) = \epsilon_{\sigma,\vec{p}}\left(n^0\left(\vec{p} + m\vec{v}\right)\right). \tag{3.56}$$

Extending this, we have

$$\begin{aligned}
\partial_{\vec{p}'} n\left(\vec{p}\right) &= \partial_{\vec{p}'}\epsilon_\sigma\left(\vec{p}'\right)\frac{\partial n^0\left(\vec{p}'\right)}{\partial\epsilon_\sigma\left(\vec{p}'\right)} \\
\epsilon'_\sigma\left(\vec{p}\right) &= \epsilon_\sigma\left(\vec{p}\right) + \frac{1}{V}\sum_{p',\sigma} f^{\mathrm{s}}_{pp'} m\vec{v}\cdot\frac{\vec{p}'}{m^*}\frac{\partial n^0\left(p'\right)}{\partial\epsilon_\sigma\left(p'\right)} \\
\epsilon'_\sigma\left(\vec{p}\right) &= \epsilon\left(p\right) - F^{\mathrm{s}}_1\frac{m}{m^*}\vec{p}\cdot\vec{v}
\end{aligned} \tag{3.57}$$

where at the Fermi surface with Fermi momentum p_{F}, we can read off from the expansion in Eq. (3.54)

$$\frac{m - m^*}{m^*} = -\frac{m}{m^*}F^{\mathrm{s}}_1 \tag{3.58}$$

which leads to the form of effective mass:

$$\frac{m^*}{m} = 1 + F^{\mathrm{s}}_1. \tag{3.59}$$

We tabulate the results in Tab. 3.2

3.3.2 Compressibility

In general, the compressibility K is related to the derivative of the chemical potential with respect to number density as:

$$\frac{1}{K} = n^2 \frac{\partial \mu}{\partial n} = \frac{1}{3} n k_{\mathrm{F}} \frac{\partial \mu}{\partial k_{\mathrm{F}}}. \tag{3.60}$$

In the case of the non-interacting Fermi gas, this gives

$$K_0 = \frac{N^*(0)}{n^2}. \tag{3.61}$$

Going back to Eq. (3.60), we see that we need to evaluate the derivative of the chemical potential with respect to the Fermi wavevector within the framework of Fermi Liquid Theory. First we recognize that μ is the energy of adding a particle to the Fermi surface. Within Fermi Liquid Theory, this is the same as the energy of the quasiparticle, which is defined already in the Landau energy functional, and thus, $\mathcal{E}_{k_{\mathrm{F}},\sigma} = \mu$. The change in the chemical potential, $\delta\mu$, as a result of adding a quasiparticle to the Fermi surface with some effective speed, v_{F}^* , is due to both the expansion of the Fermi sphere as the radius increases from k_{F} to $k_{\mathrm{F}} + \delta k_{\mathrm{F}}$ as well as the interaction energy (found through the interaction functions). Explicitly, this difference in the chemical potential takes the form

$$\delta\mu = \tilde{\mathcal{E}}_{k_{\mathrm{F}}+\delta k_{\mathrm{F}},\sigma} - \tilde{\mathcal{E}}_{k_{\mathrm{F}},\sigma} = v_{\mathrm{F}}^* \hbar \delta k_{\mathrm{F}} + \sum_{\mathbf{k}',|\mathbf{k}|=k_{\mathrm{F}},\sigma'} f_{\mathbf{k},\sigma,\mathbf{k}',\sigma'} \delta\mathcal{N}_{\mathbf{k}',\sigma'}, \tag{3.62}$$

in which $\delta\mathcal{N}_{\mathbf{k},\sigma}$ was 1 in the region of $k_{\mathrm{F}} < k < k_{\mathrm{F}} + \delta k_{\mathrm{F}}$ and 0 for all other k, because we are looking at the case of a single quasiparticle being added to a small region near the Fermi surface.

With this, we can consider the change in energy due to the quasiparticle

$$\delta\epsilon_\sigma(p) = f_0^{\mathrm{s}} - \frac{1}{V}\sigma_{\sigma',\vec{p}'}\delta n_{\sigma'}(\vec{p}') = f_s^{\mathrm{s}}\delta n \tag{3.63}$$

where

$$\delta n_\sigma(\vec{p}) = \frac{\partial n_\sigma(\vec{p})}{\partial\epsilon\sigma(\vec{p})}\left(f_0^{\mathrm{s}}\delta n - \delta\mu\right). \tag{3.64}$$

Thus we have

$$\delta n = -N(0)\left(f_0^{\mathrm{s}}\delta n - \delta\mu\right), \tag{3.65}$$

and by recalling that $F_0^{\mathrm{s}} = N(0)f_0^{\mathrm{s}}$, we have

$$\frac{\partial n}{\partial\mu} = \frac{N(0)}{1+F_0^{\mathrm{s}}}. \tag{3.66}$$

The ratio of compressibility for the interacting case K to the non-interacting case K_0 is thus

$$\frac{K}{K_0} = \frac{1}{m/m^* + mF_0^{\mathrm{s}}/m^*} \tag{3.67}$$

Generally, a positive compressibility is the condition for stability. That is, if a negative compressibility is calculated, it implies that there is an instability in forming domains of higher and lower densities in the form of phase separation.

We tabulate the results in Tab. 3.2

3.3.3 Spin Susceptibility

Spin susceptibility is in effect a response to an external magnetic field. This is generally considered in chemistry for electrons which act as moving charges, which respond to magnetic fields. A neutron does not have charge, but does have a magnetic

moment, allowing the concept of spin susceptibility to still be valid.

In fact, this can be expressed as

$$\delta\epsilon_\sigma\left(\vec{p}\right) = -\frac{1}{2}\hbar\gamma\sigma_z H + \frac{1}{V}\sum_{\sigma',\vec{p}'} f_{\sigma,\sigma'}\left(\vec{p},\vec{p}'\right)\delta n_{\sigma'}\left(\vec{p}'\right). \tag{3.68}$$

This is a very similar functional form to the above treatment for chemical potential and compressibility. Since the chemical potential is a scalar, it cannot have a linear variation with the magnetic field. The chemical potential with the magnetic field interacting Hamiltonian must be an even power of at least order 2 in H. Thus, it does not contribute to the magnetic susceptibility. Thus we can ignore this contribution. Applying the same treatment as for the compressibility above, we have that the ratio of spin susceptibility for the interacting case χ_S to the non-interacting case χ_P is

$$\frac{\chi_S}{\chi_P} = \frac{1}{m/m^* + mF_0^a/m^*} \tag{3.69}$$

We tabulate the results in Tab. 3.2

g-Factor

The ratio of the effective g-factor (which can be interpreted as being associated with the energy change that results from flipping of the spin of a single quasiparticle from down to up in the presence of the spin polarization created by a magnetic field B, without allowing that polarization to change), g^*, to g is

$$\frac{g^*}{g} = \frac{m}{m^*}\frac{\chi_S}{\chi_P}. \tag{3.70}$$

Using the relations for the spin susceptibility and effective mass, we thus have

$$\frac{g^*}{g} = \frac{1}{1+F_0^a}. \tag{3.71}$$

Of note, g-factors for excited states of nuclei can reach values higher more than 100% of the value for a free neutron.

We tabulate the results in Tab. 3.2

3.3.4 Observables for Interacting Neutron Matter

Plugging in the relevant Fermi liquid parameters into Eqs. (3.59, 3.67-3.71), we get results for the effective mass ratio, the compressibility ratio, the spin susceptibility ratio, and the g-factor ratio, which are tabulated in Tab 3.2.

Table 3.2: Observable parameters calculated from the Fermi liquid parameters obtained for $n = 0.06$ fm^{-3} neutrons interacting through the av8'+uix potential.

	Trapezoidal	Right Riemann	Left Riemann
m^*/m	0.84 ± 0.05	0.9 ± 0.1	0.79 ± 0.09
K^*/K_0	-20 ± 40	-20 ± 60	-20 ± 90
χ_S/χ_P	0.90 ± 0.07	0.9 ± 0.2	0.88 ± 0.1
g^*/g	1 ± 1	1 ± 1	1 ± 1

Beginning with the effective mass ratios, we see that for each method of integration the results agree within error. Comparing this to the literature, the parameters calculated here agree within error.

The compressiblity ratios have large errors, but for this density, the calculated value seems to be negative, which is interesting. For nucleons below the nuclear density ($n \sim 0.16$), a negative compressibility to me can be rationalized, as nuclear matter "wants" to be at the nuclear density, without any notable forces acting on it. For example, the large force of gravity in neutron stars. Thus, this negative

compressibility corresponds to an unstable state for the system. This is something that can be readily tested by exploring how the compressibility ratio changes as the density approaches and exceeds the nuclear density.

Spin susceptibility for neutron matter, is more interesting for a neutron star where the magnetic fields can be large. Though, it may also be of interest for neutron structure in general. The results for each method of integration agree within error, and compared to the compressibility ratios and g-factor ratios, have relatively small errors. The results here agree with literature values.

The g-factor ratios have errors of 100%, and the values for each method all agree within error. In the literature, the value for free neutron 3.826.

In effect, we have demonstrated a systematic way of calculating observables for neutron matter as a function of density, based on ab-initio, first principles calculations of the neutron energies.

Chapter 4

Conclusion and Outlook

In this work we applied the framework of Landau Fermi Liquid Theory to neutron matter. This framework has been largely used for electron matter, but is generalizable for fermions in general. Through modification, we applied the theory to interacting nucleons, where we gave care to the interactions involved, as we needed to justify the applicability of this framework given the non-perturbative nature of the strong force.

By using Quantum Monte Carlo calculations for the energies of the system of neutrons, we had accurate and precise energies that were used as inputs. Further, these are ab-initio calculations from first principles, which can be calculated for a fixed density.

By combining Fermi Liquid Theory and Quantum Monte Carlo methods, we were able to systematize the calculation of parameters including effective mass, compressibility, spin susceptibility, and g-factor for neutron matter at the thermodynamic limit.

This can be extended to look these observables as a function of density for neutron matter, in a straightforward manner. This motivates a study looking for implied phase transitions that can be seen in the trends formed by the observables as a function of

number density. This is particularly relevant for nuclear astrophysics, where neutron stars may be modeled as nuclear matter, with a thermodynamic number of neutrons. This can further be extended to include both protons and neutrons. However for this case, the charged nucleons will necessitate careful treatment of the observables. In particular, the calculations for spin susceptibility and compressibility will need to address the contributions from the electromagnetic interactions, rather than just the case of neutral matter.

Bibliography

[1] Zi Cai and Jinguo Liu. Approximating quantum many-body wave functions using artificial neural networks. *Phys. Rev. B*, 97:035116, Jan 2018.

[2] Stephan Humeniuk and Tommaso Roscilde. Quantum monte carlo calculation of entanglement rényi entropies for generic quantum systems. *Phys. Rev. B*, 86:235116, Dec 2012.

[3] J. Eisert, M. Friesdorf, and C. Gogolin. Quantum many-body systems out of equilibrium. *Nature Physics*, 11(2):124–130, Feb 2015.

[4] Kiel T. Williams, Yuan Yao, Jia Li, Li Chen, Hao Shi, Mario Motta, Chunyao Niu, Ushnish Ray, Sheng Guo, Robert J. Anderson, Junhao Li, Lan Nguyen Tran, Chia-Nan Yeh, Bastien Mussard, Sandeep Sharma, Fabien Bruneval, Mark van Schilfgaarde, George H. Booth, Garnet Kin-Lic Chan, Shiwei Zhang, Emanuel Gull, Dominika Zgid, Andrew Millis, Cyrus J. Umrigar, and Lucas K. Wagner. Direct comparison of many-body methods for realistic electronic hamiltonians. *Phys. Rev. X*, 10:011041, Feb 2020.

[5] Si-sheng Ou-Yang, Jun-yan Lu, Xiang-qian Kong, Zhong-jie Liang, Cheng Luo, and Hualiang Jiang. Computational drug discovery. *Acta Pharmacologica Sinica*, 33(9):1131–1140, Sep 2012.

[6] Jamelah S. Al-Otaibi, Paul Teesdale Spittle, and Tarek M. El Gogary. Interaction of anthraquinone anti-cancer drugs with dna:experimental and computational quantum chemical study. *Journal of Molecular Structure*, 1127:751–760, 2017.

[7] Zhi Wei Seh, Jakob Kibsgaard, Colin F. Dickens, Ib Chorkendorff, Jens K. Nørskov, and Thomas F. Jaramillo. Combining theory and experiment in electrocatalysis: Insights into materials design. *Science*, 355(6321), 2017.

[8] Stefano Curtarolo, Gus L. W. Hart, Marco Buongiorno Nardelli, Natalio Mingo, Stefano Sanvito, and Ohad Levy. The high-throughput highway to computational materials design. *Nature Materials*, 12(3):191–201, Mar 2013.

[9] Thomas Rauscher, Friedrich-Karl Thielemann, and Karl-Ludwig Kratz. Nuclear level density and the determination of thermonuclear rates for astrophysics. *Phys. Rev. C*, 56:1613–1625, Sep 1997.

[10] N. K. Timofeyuk, P. Descouvemont, and R. C. Johnson. Relation between proton and neutron asymptotic normalization coefficients for light mirror nuclei and its relevance for nuclear astrophysics. *The European Physical Journal A - Hadrons and Nuclei*, 27(1):269–276, Mar 2006.

[11] G. Kotliar, S. Y. Savrasov, K. Haule, V. S. Oudovenko, O. Parcollet, and C. A. Marianetti. Electronic structure calculations with dynamical mean-field theory. *Reviews of Modern Physics*, 78(3):865–951, August 2006.

[12] Lei Ying. On the approximation error of mean-field models. In *Proceedings of the 2016 ACM SIGMETRICS International Conference on Measurement and Modeling of Computer Science*, SIGMETRICS '16, page 285–297, New York, NY, USA, 2016. Association for Computing Machinery.

[13] P. Ring. Relativistic mean field theory in finite nuclei. *Progress in Particle and Nuclear Physics*, 37:193–263, 1996.

[14] Antoine Georges, Gabriel Kotliar, Werner Krauth, and Marcelo J. Rozenberg. Dynamical mean-field theory of strongly correlated fermion systems and the limit of infinite dimensions. *Rev. Mod. Phys.*, 68:13–125, Jan 1996.

[15] G. Colò. Nuclear density functional theory. *Advances in Physics: X*, 5(1):1740061, 2020.

[16] Jianwei Sun, Adrienn Ruzsinszky, and John P. Perdew. Strongly constrained and appropriately normed semilocal density functional. *Phys. Rev. Lett.*, 115:036402, Jul 2015.

[17] DAVID CEPERLEY and BERNI ALDER. Quantum monte carlo. *Science*, 231(4738):555–560, 1986.

[18] James Shee, Shiwei Zhang, David R. Reichman, and Richard A. Friesner. Chemical transformations approaching chemical accuracy via correlated sampling in auxiliary-field quantum monte carlo. *Journal of Chemical Theory and Computation*, 13(6):2667–2680, Jun 2017.

[19] D. M. Ceperley and B. J. Alder. Ground state of the electron gas by a stochastic method. *Phys. Rev. Lett.*, 45:566–569, Aug 1980.

[20] Ashley Montanaro. Quantum speedup of monte carlo methods. *Proceedings of the Royal Society A: Mathematical, Physical and Engineering Sciences*, 471(2181):20150301, 2015.

[21] Omar Valsson and Claudia Filippi. Photoisomerization of model retinal chromophores: Insight from quantum monte carlo and multiconfigurational perturbation theory. *Journal of Chemical Theory and Computation*, 6(4):1275–1292, Apr 2010.

[22] Andrea Zen, Sandro Sorella, Michael J. Gillan, Angelos Michaelides, and Dario Alfè. Boosting the accuracy and speed of quantum monte carlo: Size consistency and time step. *Phys. Rev. B*, 93:241118, Jun 2016.

[23] Emanuele Coccia, Daniele Varsano, and Leonardo Guidoni. Theoretical s1 ← s0 absorption energies of the anionic forms of oxyluciferin by variational monte carlo and many-body green's function theory. *Journal of Chemical Theory and Computation*, 13(9):4357–4367, Sep 2017.

[24] Jeremy McMinis, Raymond C. Clay, Donghwa Lee, and Miguel A. Morales. Molecular to atomic phase transition in hydrogen under high pressure. *Phys. Rev. Lett.*, 114:105305, Mar 2015.

[25] Andrea Zen, Jan Gerit Brandenburg, Jiří Klimeš, Alexandre Tkatchenko, Dario Alfè, and Angelos Michaelides. Fast and accurate quantum monte carlo for molecular crystals. *Proceedings of the National Academy of Sciences*, 115(8):1724–1729, 2018.

[26] Miguel A. Morales, John R. Gergely, Jeremy McMinis, Jeffrey M. McMahon, Jeongnim Kim, and David M. Ceperley. Quantum monte carlo benchmark of exchange-correlation functionals for bulk water. *Journal of Chemical Theory and Computation*, 10(6):2355–2362, Jun 2014.

[27] Luke Shulenburger and Thomas R. Mattsson. Quantum monte carlo applied to solids. *Phys. Rev. B*, 88:245117, Dec 2013.

[28] Ingo Tews. Quantum monte carlo methods for astrophysical applications. *Frontiers in Physics*, 8:153, 2020.

[29] Michael McNeil Forbes, Sukanta Bose, Sanjay Reddy, Dake Zhou, Arunava Mukherjee, and Soumi De. Constraining the neutron-matter equation of state with gravitational waves. *Phys. Rev. D*, 100:083010, Oct 2019.

[30] J. Carlson, S. Gandolfi, F. Pederiva, Steven C. Pieper, R. Schiavilla, K. E. Schmidt, and R. B. Wiringa. Quantum Monte Carlo methods for nuclear physics. *Reviews of Modern Physics*, 87(3):1067–1118, September 2015. arXiv: 1412.3081.

[31] J.E. Lynn, I. Tews, S. Gandolfi, and A. Lovato. Quantum monte carlo methods in nuclear physics: Recent advances. *Annual Review of Nuclear and Particle Science*, 69(1):279–305, 2019.

[32] R. B. Wiringa, V. G. J. Stoks, and R. Schiavilla. Accurate nucleon-nucleon potential with charge-independence breaking. *Physical Review C*, 51(1):38–51, January 1995.

[33] J. Carlson and R. Schiavilla. Structure and dynamics of few-nucleon systems. *Rev. Mod. Phys.*, 70:743–841, Jul 1998.

[34] R. B. Wiringa and Steven C. Pieper. Evolution of Nuclear Spectra with Nuclear Forces. *Physical Review Letters*, 89(18):182501, October 2002. arXiv: nucl-th/0207050.

[35] Steven C. Pieper, V. R. Pandharipande, R. B. Wiringa, and J. Carlson. Realistic models of pion-exchange three-nucleon interactions. *Physical Review C*, 64(1):014001, June 2001. arXiv: nucl-th/0102004.

[36] Sonia Bacca and Saori Pastore. Electromagnetic reactions on light nuclei. *arXiv:1407.3490 [nucl-ex, physics:nucl-th]*, July 2014. arXiv: 1407.3490.

[37] Kimiko Sekiguchi. Experimental Approach to Three-Nucleon Forces via Few-Nucleon Scattering. *Few-Body Systems*, 60(3):56, August 2019.

[38] Z. Asadi Aghbolaghi and M. Bigdeli. Argonne family potentials and neutron star matter equation of state. *The European Physical Journal Plus*, 134(9):430, September 2019.

[39] Giuseppe Carleo and Matthias Troyer. Solving the Quantum Many-Body Problem with Artificial Neural Networks. *Science*, 355(6325):602–606, February 2017. arXiv: 1606.02318.

[40] Scott Bogner, Aurel Bulgac, Joseph A. Carlson, Jonathan Engel, George Fann, Richard J. Furnstahl, Stefano Gandolfi, Gaute Hagen, Mihai Horoi, Calvin W. Johnson, Markus Kortelainen, Ewing Lusk, Pieter Maris, Hai Ah Nam, Petr Navratil, Witold Nazarewicz, Esmond G. Ng, Gustavo P. A. Nobre, Erich Ormand, Thomas Papenbrock, Junchen Pei, Steven C. Pieper, Sofia Quaglioni, Kenneth J. Roche, Jason Sarich, Nicolas Schunck, Masha Sosonkina, Jun Terasaki, Ian J. Thompson, James P. Vary, and Stefan M. Wild. Computational Nuclear Quantum Many-Body Problem: The UNEDF Project. *Computer Physics Communications*, 184(10):2235–2250, October 2013. arXiv: 1304.3713.

[41] Stephen Wiesner. Simulations of Many-Body Quantum Systems by a Quantum Computer. *arXiv:quant-ph/9603028*, March 1996. arXiv: quant-ph/9603028.

[42] G. Vidal. Efficient simulation of one-dimensional quantum many-body systems. *Physical Review Letters*, 93(4):040502, July 2004. arXiv: quant-ph/0310089.

[43] Alexander G Ushveridze. *Quasi-exactly solvable models in quantum mechanics*. Routledge, 2017.

[44] Alexandros Gezerlis and G. F. Bertsch. Effective 3-Body Interaction for Mean-Field and Density-Functional Theory. August 2010.

[45] N. D. Drummond, Bartomeu Monserrat, Jonathan H. Lloyd-Williams, P. López Ríos, Chris J. Pickard, and R. J. Needs. Quantum monte carlo study of the phase diagram of solid molecular hydrogen at extreme pressures. *Nature Communications*, 6(1):7794, 2015.

[46] Juan A. Santana, Jaron T. Krogel, Jeongnim Kim, Paul R. C. Kent, and Fernando A. Reboredo. Structural stability and defect energetics of zno from diffusion quantum monte carlo. *The Journal of Chemical Physics*, 142(16):164705, 2015.

[47] Chandrima Mitra, Jaron T. Krogel, Juan A. Santana, and Fernando A. Reboredo. Many-body ab initio diffusion quantum monte carlo applied to the strongly correlated oxide nio. *The Journal of Chemical Physics*, 143(16):164710, 2015.

[48] Kayahan Saritas, Tim Mueller, Lucas Wagner, and Jeffrey C. Grossman. Investigation of a quantum monte carlo protocol to achieve high accuracy and

high-throughput materials formation energies. *Journal of Chemical Theory and Computation*, 13(5):1943–1951, 2017. PMID: 28358499.

[49] James Shee, Benjamin Rudshteyn, Evan J. Arthur, Shiwei Zhang, David R. Reichman, and Richard A. Friesner. On achieving high accuracy in quantum chemical calculations of 3d transition metal-containing systems: A comparison of auxiliary-field quantum monte carlo with coupled cluster, density functional theory, and experiment for diatomic molecules. *Journal of Chemical Theory and Computation*, 15(4):2346–2358, 2019. PMID: 30883110.

[50] J. Emiliano Deustua, Ilias Magoulas, Jun Shen, and Piotr Piecuch. Communication: Approaching exact quantum chemistry by cluster analysis of full configuration interaction quantum monte carlo wave functions. *The Journal of Chemical Physics*, 149(15):151101, 2018.

[51] Matúš Dubecký, Petr Jurečka, Lubos Mitas, Matej Ditte, and Roman Fanta. Toward accurate hydrogen bonds by scalable quantum monte carlo. *Journal of Chemical Theory and Computation*, 15(6):3552–3557, 2019. PMID: 31026158.

[52] Yuan Liu, Minsik Cho, and Brenda Rubenstein. Ab initio finite temperature auxiliary field quantum monte carlo. *Journal of Chemical Theory and Computation*, 14(9):4722–4732, 2018. PMID: 30102856.

[53] Stefano Gandolfi, Alexandros Gezerlis, and J. Carlson. Neutron Matter from Low to High Density. *Annual Review of Nuclear and Particle Science*, 65(1):303–328, October 2015. arXiv: 1501.05675.

[54] J. Carlson, S. Gandolfi, F. Pederiva, Steven C. Pieper, R. Schiavilla, K. E. Schmidt, and R. B. Wiringa. Quantum monte carlo methods for nuclear physics. *Rev. Mod. Phys.*, 87:1067–1118, Sep 2015.

[55] D. Lonardoni, J. Carlson, S. Gandolfi, J. E. Lynn, K. E. Schmidt, A. Schwenk, and X. B. Wang. Properties of nuclei up to $a = 16$ using local chiral interactions. *Phys. Rev. Lett.*, 120:122502, Mar 2018.

[56] Jun S. Liu. Metropolized independent sampling with comparisons to rejection sampling and importance sampling. *Statistics and Computing*, 6(2):113–119, June 1996.

[57] Peter W. Glynn and Donald L. Iglehart. Importance sampling for stochastic simulations. *Management Science*, 35(11):1367–1392, 1989.

[58] Nicholas Metropolis, Arianna W. Rosenbluth, Marshall N. Rosenbluth, Augusta H. Teller, and Edward Teller. Equation of state calculations by fast computing machines. *The Journal of Chemical Physics*, 21(6):1087–1092, 1953.

[59] Philipp Bader, Sergio Blanes, and Fernando Casas. Solving the Schr\"odinger eigenvalue problem by the imaginary time propagation technique using splitting methods with complex coefficients. *The Journal of Chemical Physics*, 139(12):124117, September 2013. arXiv: 1304.6845.

[60] R J Needs, M D Towler, N D Drummond, and P López Ríos. Continuum variational and diffusion quantum Monte Carlo calculations. *Journal of Physics: Condensed Matter*, 22(2):023201, January 2010.

[61] W. M. C. Foulkes, L. Mitas, R. J. Needs, and G. Rajagopal. Quantum Monte Carlo simulations of solids. *Reviews of Modern Physics*, 73(1):33–83, January 2001.

[62] Matthias Troyer and Uwe-Jens Wiese. Computational Complexity and Fundamental Limitations to Fermionic Quantum Monte Carlo Simulations. *Physical Review Letters*, 94(17), May 2005.

[63] C. J. Umrigar, M. P. Nightingale, and K. J. Runge. A diffusion monte carlo algorithm with very small time-step errors. *The Journal of Chemical Physics*, 99(4):2865–2890, 1993.

[64] G. Senatore and N. H. March. Recent progress in the field of electron correlation. *Reviews of Modern Physics*, 66(2):445–479, April 1994.

[65] S. Gandolfi, F. Pederiva, S. Fantoni, and K. E. Schmidt. Auxiliary field diffusion monte carlo calculation of nuclei with $a \leq 40$ with tensor interactions. *Phys. Rev. Lett.*, 99:022507, Jul 2007.

[66] A. Sarsa, S. Fantoni, K. E. Schmidt, and F. Pederiva. Neutron matter at zero temperature with an auxiliary field diffusion monte carlo method. *Phys. Rev. C*, 68:024308, Aug 2003.

[67] G. Ortiz, D. M. Ceperley, and R. M. Martin. New stochastic method for systems with broken time-reversal symmetry: 2d fermions in a magnetic field. *Phys. Rev. Lett.*, 71:2777–2780, Oct 1993.

[68] Robert Jastrow. Many-body problem with strong forces. *Phys. Rev.*, 98:1479–1484, Jun 1955.

[69] Mateusz Buraczynski, Nawar Ismail, and Alexandros Gezerlis. Neutron matter at the interface(s): from interactions to ab initio and from there to phenomenology. *arXiv:1906.01674 [astro-ph, physics:cond-mat, physics:nucl-th]*, June 2019. arXiv: 1906.01674.